Turbo Hybrid Automatic Repeat reQuest (HARQ)

By Ade Irawan

A thesis submitted to
School of Information Science,
Japan Advanced Institute of Science and Technology,
in partial fulfillment of the requirements
for the degree of
Master of Information Science
Graduate Program in Information Science

Written under the direction of
Professor Tad Matsumoto

March, 2013

Turbo Hybrid Automatic Repeat reQuest (HARQ)

By Ade Irawan (1010203)

A thesis submitted to
School of Information Science,
Japan Advanced Institute of Science and Technology,
in partial fulfillment of the requirements
for the degree of
Master of Information Science
Graduate Program in Information Science

Written under the direction of
Professor Tad Matsumoto

and approved by
Professor Tad Matsumoto
Professor Mineo Kaneko
Associate Professor Kiyofumi Tanaka

February, 2013 (Submitted)

I certify that I have prepared this Master's Thesis by myself without any inadmissible outside help.

Ade Irawan
JAIST, 6 February 2013

Author : _____

Date : _____

Supervisor : _____

Acknowledgments

First of all, I thank to God for His bless and merciful throughout all of my life. Then, I would like to express my sincerest gratitude to my supervisor Professor Tadashi Matsumoto, commonly called Tad, for his guidance and insights throughout this thesis and my education at JAIST. His engineering intuition and experience inspired my interest in ARQ and guided my research. I am extremely grateful to him for all his ultra-prompt help and for his numerous proofreads that greatly improved my research work. This thesis would not have been possible without his guidance.

I wish to thank Dr. Khoirul Anwar who is the Tad's Assistant Professor during my education at JAIST. His enthusiasm for research enabled me to work on this thesis. I deeply appreciate his insightful ideas and his many hours spent with me discussing my research.

I wish to thank my labmates for their help and friendship, including Kisho Fukawa, Yace Takano, Henry, Simon, Xiaobo, Zhou Hui, Pen Shun, Valtteri, Xin, Wu, Ken, Ricardo, Reza. Our lab. has been a great environment, thanks to such a group of highly talented people.

This research was partially supported by Sanyo and Japanese Government Scholarship. I thank to them for giving me chances to pursue my master degree and researches, and supports during my stay in Japan.

Finally, I would like to express special thanks to my family. I thank my parents for their love, help and encouragement which made it possible for me to get a master degree. No words are enough to show my appreciation for them. My wife Laili Mutiara has always supported me during my last one year at JAIST. Her true love and extreme patience have made this thesis possible. I greatly appreciate their thoughtful support.

Achievements

Journal Paper

1. A. Irawan, K. Anwar, T. Matsumoto, "Low Complexity Time Concatenated Turbo Equalization for Block Transmission without Guard Interval: Part 3 Application to Multiuser SIMO-OFDM", Wireless Personal Communication, Springer, July 2012

2. A. Irawan, K. Anwar, T. Matsumoto, "Combining-after-Decoding Turbo Hybrid ARQ by Utilizing Doped-Accumulator", IEEE Communication Letters, October 2012 - *under review*

Oral Presentation

1. M. Cheng, A. Irawan, K. Anwar, T. Matsumoto, "BICM-ID for Relay System Allowing Intra-link Errors and a Similarity Constellation to ARQ Schemes", Progress In Electromagnetics Research Symposium (PIERS), Kuala Lumpur, Malaysia, 27-30 March 2012 (peer-reviewed)

2. A. Irawan, K. Anwar, T. Matsumoto,"Chained Turbo Equalization for OFDM System without Guard Interval", IEICE2011, Tokyo, Japan, March 2011

Poster Presentation

1. A. Irawan, K. Anwar, T. Matsumoto , "Chained Turbo Equalization for Multiuser SIMO-OFDM Systems without Cyclic Prefix", ITG-WSA 2012, Dresden, Germany, 7-8March 2012 (peer-reviewed)

2. A. Irawan, K. Anwar, T. Matsumoto , "Chained Turbo Equalization for Block Transmission without Guard Interval and Its Application", Wireless Information Theory Summer School, 27-29 July 2012 (not peer-reviewed)

Abstract

This thesis proposes an efficient decoding strategy for turbo hybrid automatic repeat request (Turbo HARQ). With the new strategy of HARQ protocol based on the turbo principle, it is made possible to combine and decode all (re)transmitted packets in an iterative way. In general, two packet combining schemes are applicable for HARQ: combining-before-decoding (CBD) which is based on the retransmission of the same coded bits, and combining-after-decoding (CAD) which is based on the retransmission of additional redundancy bits produced from an interleaved information version of sequence.

This thesis first examines the basic properties of CAD and CBD, and then derives the theoretical limit of the both techniques. It is shown that CAD outperforms CBD. Based on the theoretical limit comparison, this thesis proposes a doped-accumulator assisted CAD technique (ACC-CAD) with different doping rate per transmission phases for practical application. The proposed CAD performs vertical iterations (*VI*) between the decoders of the parallel-concatenated code (PCC) where extrinsic log-likelihood ratio (LLR) of the uncoded bits are exchanged via *VI*. The doped-accumulator enables the two extrinsic information transfer (EXIT) curves of the equalizer and the joint decoders to match very well and the convergence tunnel to open until a point very close to the (1.0,1.0) mutual information point.

For fair comparison, this thesis considers the latest CBD technique, presented in a literature, that combines all path energies of the received signals to achieve full diversity gain at the receiver, and then the decoding of the serial concatenated code is performed via horizontal iterations (*HI*s). This thesis also provides the decoding complexity comparison between the ACC-CAD and the CBD.

Finally, excellent performance of the ACC-CAD is verified through EXIT analysis as well as bit-error-rate (BER), frame-error-rate (FER), and throughput performances via computer simulations.

In addition, this thesis also shows the excellent performance of frequency domain soft cancellation and minimum mean square error (FD-SC/MMSE) equalization, applied in to all the Turbo HARQ systems evaluated in this thesis in multipath fading channels, where guard interval is not used in all transmitted symbols.

Table of Contents

List of Figures

List of Tables

Abbreviations

ACC-CAD	Doped-accumulator assisted Combining-After-Decoding
ACK	Acknowledgment
ARQ	Automatic Repeat reQuest
AWGN	Additive White Gaussian Noise
BER	Bit Error Rate
BPSK	Binary Phase Shift Keying
CAD	Combining After Decoding
CBD	Combining Before Decoding
CC	Chase Combining
CHATUE	Chained Turbo Equalization
CIR	Channel Impulse Response
CP	Cyclic Prefix
CRC	Cyclic Redundancy Check
$DAcc$	Doped-Accumulator
D_{DAcc}	Decoder of $DAcc$
DFT	Discrete Fourier Transform
EQ	Equalizer
EXIT	Extrinsic Information Transfer
FD-SC/MMSE	Frequency-Domain Soft Cancellation and Minimum Mean Squared Error
FEC	Forward Error Correction

FER	Frame Error Rate
GI	Guard Interval
HARQ	Hybrid ARQ
HI	Horizontal Iteration
IBI	Inter-Block Interference
ICI	Inter-Carrier Interference
IDFT	Inverse Discrete Fourier Transform
IEQ	Integrated Equalization
i.i.d.	independent and identically distributed
IR	Incremental Redundancy
ISI	Inter-Symbol Interference
LLR	Log Likelihood Ratio
MAP	Maximum a Posteriori
MI	Mutual Information
MIMO	Multiple-Input Multiple-Output
MU-SIMO-OFDM	Multiuser-SIMO-OFDM
NACK	Negative Acknowledgment
NSNRCC	Non-systematic Non-recursive Convolutional Code
OFDM	Orthogonal Frequency Division Multiplexing
PCC	Parallel Concatenated Code
PSI	Parity Spreading Interleaver
RSCC	Recursive Systematic Convolutional Code
SCC	Serial Concatenated Code
SIMO	Single-Input Multiple-Output
SNR	Signal-to-Noise Ratio
TDT	Turbo Diversity Transmission
VI	Vertical Iteration

Chapter 1

Introduction

1.1 Motivation

None of data communication systems is absolutely reliable in practice because of noise, distortions, interferences, or other forms of impairments. Therefore, the systems need error control strategies in order to detect or to correct errors occurring in the transmission process. Controlling transmission errors in data communication systems can be performed by using either automatic-repeat-request (ARQ) or forward-error-correction (FEC) techniques [1].

In ARQ schemes, the purpose of adding redundancy is for error detection, and retransmission is performed upon requested. Hence, it is simple to be implemented. However, a severe drawback of ARQ systems is that its throughput efficiency decreases rapidly with increasing channel-error rate, because more retransmissions are requested with lower channel quality.

On the other hand, in communication systems where feedback channel is not available and hence retransmission request is not possible, the system has to use error-correcting codes appropriate to the operational point of signal-to-noise power ratio (SNR), to combat transmission errors. The throughput efficiency of FEC systems can be maintained constant which is equal to the code rate, given the operational point of SNR. However, this advantage arises only when the received SNR is known to the transmitter side. Furthermore, it is difficult to adjust the code parameters, if channel is time varying. Hence, ARQ is often preferred in data communication systems, for instance computer communication networks, if feedback channel is available. On the contrary, FEC is preferred when feedback channel is not available.

Hybrid ARQ (HARQ) schemes exploit the beneficial points of the both ARQ and FEC to overcome their drawbacks. HARQ systems do not discard the unsuccessful results of FEC decoding, but aims to combine it with the frame to be retransmitted. Hence, the larger the error correction capability, the more the retransmission performed, and thereby HARQ can adequately adjust the total code rate, and increases the throughput of the system, as a whole, without the knowledge of the received SNR at the transmitter side. When error(s) is(are) detected in the information part after FEC decoding, the receiver requests retransmission instead of passing the unreliably decoded message to the user or data sink. Therefore, HARQ system provides higher reliability than an FEC system alone and higher throughput than the system with ARQ only.

One way to improving the reliability of FEC is by exchanging the soft information among the decoders. Exchanging soft information in an iterative (turbo) fashion for packet combining in HARQ systems has been intensively investigated in the last decade. Since C. Berrou, A. Glavieux, and P. Thitimajshima discovered the Turbo Codes in 1993 [2], it has been at a center of communication systems research. The turbo code not only offers near Shannon's limit performance, but also introduces a new approach to the design of communication systems, referred to as *turbo principle*.

The turbo principle is a general idea of combining decoding and detection where signal processing is integrated in an iterative structure. The turbo principle comprises the following aspects:

- serial and/or parallel concatenation of the communication chain components,
- soft-in soft-out decoding and/or detection,
- interleaving between the components, and
- extrinsic information exchange between the components in the form of probability or log-likelihood ratio (LLR)

Reference [3] first introduces the utilization of the turbo encoder structure in HARQ. The HARQ system forms parallel concatenation of multiple turbo codes, which is corresponding to multiple transmissions of the same information, if random interleaving is performed in the parallel branches of the encoder. At the receiver side, the packet combining-after-decoding (CAD) is performed to exploit the soft information expressed

in the form of *a priori* LLR of the uncoded (systematic) bits obtained in the last transmission for decoding the current transmission. It is shown in [3] that a considerable frame-error-rate (FER) performance gain can be achieved over conventional ARQ without packet combining.

The CAD concept has been adopted in various forms that can be found in the literatures. Reference [4] exploits the structure of [3] by replacing the turbo code in [3] with systematic recursive convolutional code. In the technique shown in [4], only either systematic or parity bits are retransmitted, and hence a considerable throughput improvement can be achieved. Reference [5] considers rate compatible punctured turbo coded HARQ to provide higher throughput. A similar technique is proposed in [6], where the parity spreading interleaver (PSI) is employed to re-order the parity bits as a scheme for flexible puncturing.

An alternative way to packet combining in the framework of ARQ in multipath propagation environment is combining-before-decoding (CBD). The CBD technique combines all path energies of the transmitted signals to achieve diversity gain at the receiver. CBD can be performed by joint soft equalization and packet combining using a maximum *a posteriori* (MAP) equalizer, as introduced in [7]. The algorithm is an extension of the well-known turbo equalization to a single-input multiple-output (SIMO) channel where signal samples, received in each retransmission phase, are stored and combined by the turbo equalizer; this concept is referred to as integrated equalization (IEQ) in [7]. The same idea for packet combining by using MAP equalization is also proposed in [8]. Although the MAP algorithm can achieve the optimal performance, its computational complexity increases exponentially with the channel memory length, and hence its capability is limited to the channel having only a few multipath components.

Another form of CBD is combining the interleaved LLRs of equalizers outputs, known as turbo-diversity transmission (TDT) presented in [9] or bit-interleaving diversity (BID) in [10]. Reference [9] introduces an improved turbo-diversity scheme to IEQ by exploiting different interleavers in every retransmission to reduce the Euclidean distance dispersion. As for IEQ, retransmission of the same codeword with an identical interleaver for every retransmission achieves only a path diversity.

It can easily be expected that in frequency-selective fading channels, the both CAD and CBD techniques can achieve a diversity order of (*number of path in the channel*) $\times$ (*transmission times*). On the top of the diversity gain, the both techniques can achieve coding gain, however the gain depends on the used coding technique, which

invokes a question that which of CAD or CBD outperforms the other. To answer this question is the major goal of this thesis.

1.2 Thesis Content

The rest of this thesis is organized as follows. The system and the channel models assumed throughout the thesis are provided in **Chapter 2**, where we also describe the turbo equalization that is used commonly in multipath fading channels. In the case of insufficient guard interval (GI), we introduce chained turbo equalization (CHATUE) algorithm that can be implemented for single carrier or orthogonal frequency division multiplexing (OFDM) systems. Furthermore, the extrinsic-information-transfer (EXIT) Chart is introduced as an useful tool to analyse the convergence property of turbo equalization and turbo decoding, also in Chapter 2.

Chapter 2 then introduces the packet combining techniques for Turbo HARQ. We derive and compare the capacities of those techniques. The outage probabilities of the systems, which is the probability that the transmission rate is lower than the capacity because of fading, are evaluated through Monte-Carlo simulations instead of numerical integral that appears in the mathematical outage expression. The obtained outage probability is used as the theoretical limits for FER performance comparison in Chapter 4.

Chapter 3 is dedicated to describing the proposed turbo HARQ scheme, ACC-CAD. We show the beneficial points of introducing doped-accumulator ($DAcc$) in ACC-CAD through EXIT analyses. **Chapter 4** also contains the simulation results and analyses of BER, FER, and throughput performances over both additive white Gaussian noise (AWGN) and multipath fading channels. At the end of this chapter, we show computational complexity analysis of evaluated systems, including our proposed system.

Finally, **Chapter 5** concludes this thesis by summarizing the major contributions and also highlighting important open research problems and directions for the future research work.

It should be noted that the chapters covering the issues of HARQ, in common use the frequency domain soft cancellation minimum mean square error (FD-SC/MMSE) equalization for single carrier cyclic prefix (CP) transmission. The CHATUE algorithm, as briefly introduced in Chapter 2, eliminates the necessity of the CP transmission, of

which research has been funded in part by SANYO Electric Co., Ltd and in part by Kinki Mobile Radio Center Inc. for OFDM application. In the main body of this thesis, we use the FD-SC/MMSE equalization technique for single carrier signalling, but it is very close to the CHATUE algorithm for OFDM. Therefore, CHATUE algorithm for OFDM is detailed only in Appendices.

Chapter 2

Turbo HARQ System Model

HARQ system consists of FEC subsystems contained within the ARQ system. Therefore, we can exploit FEC's error correction capability to improve the reliability of the system while also use a standard ARQ protocol to enhance the throughput. The turbo HARQ terminology in this thesis is interpreted as an error control system that combines (re)transmitted packets within an iterative signal detection/decoding. Hence, the FEC should not necessary be a Turbo Code as proposed in [3].

The following notations are adopted in this thesis. Vectors are expressed with bold lowercase, matrices with bold uppercase, and scalars with standard text notation. $\bullet^H$, $tr(\bullet)$, and $(\bullet)^T$ denote the Hermitian (tranpose-conjugate), the trace and the transpose operation of matrix $\bullet$, respectively. $\otimes$ denotes the Kronecker product operator. The estimation of a variable is indicated by $\hat{\bullet}$, and expectation of random variable by $\mathbf{E}[\cdot]$. An $N \times N$ identity matrix is written as $\mathbf{I}_N$, all-one $N \times M$ matrix as $\mathbf{1}_{N\times M}$, all-zero $N \times N$ matrix as $\mathbf{0}_N$, and N-point discrete Fourier transform (DFT) is denoted by $\mathbf{F}_N$.

In the framework of ARQ, the common notations, unless specified, are given in the following. The total number of transmission of the same packet is denoted by K. Hence, the total number of retransmission is $K-1$. The length of a block is denoted by N. Furthermore, we use interchangeably between block, frame, and packet.

2.1 Forward Error Correction

FEC appends redundancy when encoding a message so that the receiver can correct the errors occurring during the process of transmission. Another purpose of adding

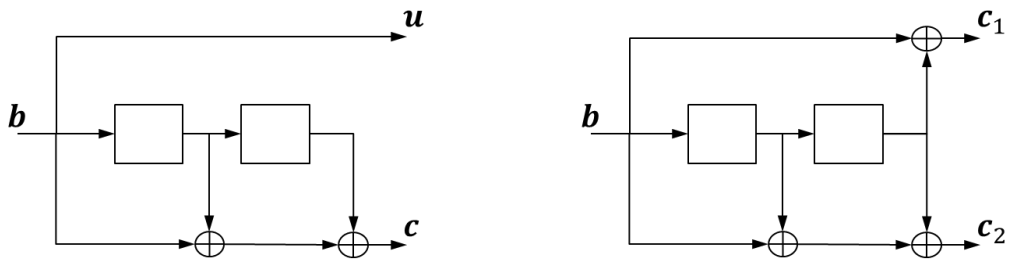

(a) Systematic Convolutional Codes (b) Non-systematic Convolutional Codes

Figure 2.1. Convolutional Codes with Memory 2

the redundancy is to detect errors, when number of errors in a packet exceeds the FEC's error correction capability. FEC can be classified into two types: convolutional codes and block codes. In practice, block codes are used for error detection, such as cyclic redundancy code (CRC), and convolutional codes are used for error correction in HARQ. The both maps information block of length k to code blocks of length n; k/n is referred to as code rate; for HARQ packet encoding, block encoding is first performed, and then convolutional encoding performed for error detection and correction, respectively. Hence, HARQ packet is composed of a concatenation of high rate block code and convolutional code with arbitary rate.

2.1.1 Convolutional Codes

Convolutional codes are commonly specified by three parameters: number of input bits k, number of output bits n, and number of memory m. We can specify a code by parameters (n, k, L), where L is called the constraint length of the code and is defined by $L = m+1$. Moreover, a measure of the efficiency of the code, code rate, is denoted by k/n.

The error correcting codes can further be classified into two categories: systematic and non-systematic codes. The systematic codes contain the information part to be transmitted in the codeword, while non-systematic codes do not, but only those bits derived from the information part is contained in the codewords. Block diagrams exemplifying systematic and non-systematic convolutional codes are shown in Fig. 2.1. In this thesis, the both systematic and non-systematic convolutional codes are used.

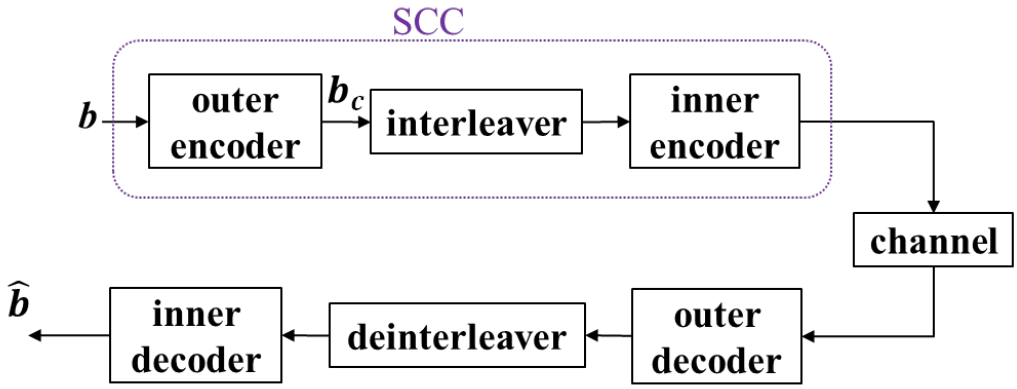

Figure 2.2. Communication System with Serial Concatenated Code

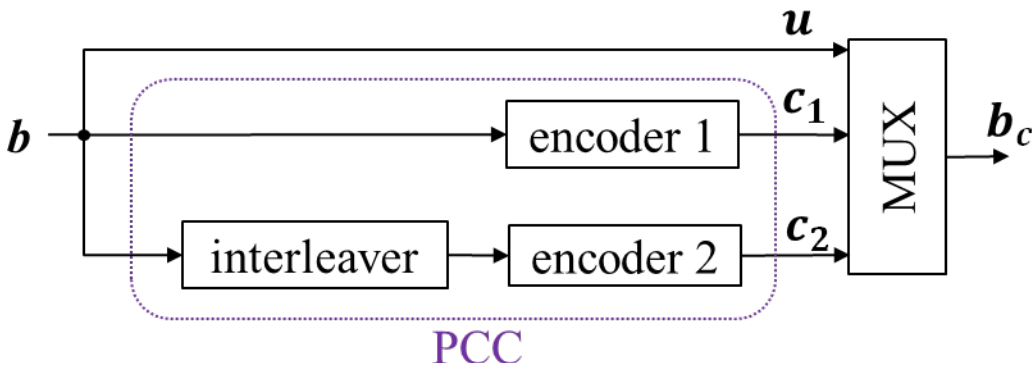

Figure 2.3. Turbo Encoder with Parallel Concatenated Code

2.1.2 Concatenated Codes

2.1.2.1 Turbo Encoding

Concatenated coding was first proposed by Forney in 1965 [11]. The conventional concatenated code is a simple cascade of Reed-Solomon (RS) code and convolutional code. It is designed for correcting both burst errors with the help of RS code and random errors with the help of convolutional code. The block diagram of this serially concatenated code (SCC) is shown in Fig. 2.2. The inner code protects the data by correcting random errors. However, some errors may still remain so that the outer code provides protection against these errors. These errors typically occur in burst so that the RS code is suitable to correct burst errors. The parallel concatenated code (PCC) as shown in Fig. 2.3 is another concatenated code. The parallel codeword is obtained from the first code by interleaving the information part, and then encoded by

the second encoder. The Turbo Codes discovered by Berrou *et.al.* in 1993 [2] is an example of PCC where recursive systematic convolutional codes (RSCCs) are used as the constituent encoders. With the conventional turbo encoder, the information bit sequence b is directly encoded by RSCC 1 and its interleaved version is encoded by RSCC 2. Hence, the systematic bits $\mathbf{b}$ are transmitted, as denoted by $\mathbf{u}$ in Fig. 2.3. The parity bits $\mathbf{c}_1$ and $\mathbf{c}_2$, produced by RSCC 1 and RSCC 2, respectively, may be fully transmitted or transmitted after puncturing to obtain higher rate codes.

Designing appropriate concatenation of codes is quite difficult. The codes are not necessarily identical. In particular, the relative capabilities of all concatenated codes need to be carefully balanced; inappropriate code concatenation may even deteriorate the BER performance because of the mismatch in their convergence properties. Moreover, the design of interleaver is an important issue, however, it is not discussed in this thesis. One way to achieve an excellent concatenated code in the framework of turbo encoding is by examining the convergence behaviour of iterative decoding with the help of EXIT chart that will be explained in Subsection 2.1.3.

2.1.2.2 Turbo Decoding

The soft information exchanged between the constituent decoders in the iterative (turbo) decoding can be represented by LLR or soft bit. The LLR of the binary variable x_n with elements $\{0, 1\}$, mapped to $\{+1, -1\}$, respectively, is given by

$$L(x_n) = \ln \frac{P(x_n = +1)}{P(x_n = -1)}, \tag{2.1}$$

with $P(x_n = +1) + P(x_n = -1) = 1$, which leads to

$$P(x_n = \pm 1) = \frac{e^{\pm L(x_n)/2}}{e^{+L(x_n)/2} + e^{-L(x_n)/2}}. \tag{2.2}$$

Hence, the sign of the $L(x_n)$ indicates whether the bit is more likely to be $+1$ or -1, and the magnitude $|L(x_n)|$ represents the reliability of the decision. n is the bit index of the coded/uncoded sequence, where coded/uncoded depends on the structure of the decoder.

The core of the iterative decoding is the use of an algorithm that computes the reliability value of coded and/or uncoded bits in each decoder which is represented by *a posteriori* probability. The *a posteriori* probability of the bit x_n output from the

decoder given input sequence $\mathbf{y}$ is expressed as

$$L_p(x_n|\mathbf{y}) = \ln \frac{P(x_n = +1|\mathbf{y})}{P(x_n = -1|\mathbf{y})} \tag{2.3}$$

$$= \ln \frac{P(\mathbf{y}|x_n = +1)\, P(x_n = +1)}{P(\mathbf{y}|x_n = -1)\, P(x_n = -1)} \tag{2.4}$$

$$= \ln \frac{P(\mathbf{y}|x_n = +1)}{P(\mathbf{y}|x_n = -1)} + \ln \frac{P(x_n = +1)}{P(x_n = -1)} \tag{2.5}$$

$$L_p(x_n|\mathbf{y}) = L(\mathbf{y}|x_n) + L_a(x_n), \tag{2.6}$$

where $L_a(x_n) = \ln \frac{P(x_n=+1)}{P(x_n=-1)}$ is the *a priori* LLR of the bit x_n, and $L(\mathbf{y}|x_n) = \ln \frac{P(\mathbf{y}|x_n=+1)}{P(\mathbf{y}|x_n=-1)}$ is the soft output of the channel. This equation corresponds to the information flow in a signal detector. By providing a constituent decoder with the *a priori* LLR, the output from another constituent decoder, is expressed as

$$L(\hat{x}_n) = L(\hat{x}'_n) + L_e(x_n), \tag{2.7}$$

where $L(\hat{x}'_n) \equiv L_p(x_n|\mathbf{y})$ denotes the soft input of the decoder, and $L_e(x_n)$ denotes the extrinsic information that represents extra knowledge achieved by another constituent decoder. Hence, the LLR $L(\hat{x}'_n)$ of a bit x_n is either monotonically increasing or decreasing, depending on the sign of x_n.

For the first iteration of decoding, we generally assume the binary data to be equally likely, yielding an initial a priori LLR value $L_a = 0$. The channel LLR value is measured by the following algorithm. If we assume that the x_n is transmitted over a Gaussian or fading channel using BPSK modulation, the probability of the signal detector or matched filter y_n, given x_n, is expressed as

$$P(y_n|x_n = \pm 1) = \frac{1}{\sigma\sqrt{2\pi}} \exp(-\frac{E_b}{2\sigma^2}(y_n \mp a)^2), \tag{2.8}$$

where E_b denotes the transmitted energy per bit, σ^2 denotes the noise variance, and a denotes the fading amplitude where $a = 1$ for AWGN channel. Therefore,

$$L(y_n|x_n) = \ln \frac{P(y_n|x_n = +1)}{P(y_n|x_n = -1)} \tag{2.9}$$

$$= \ln \frac{\exp(-\frac{E_b}{2\sigma^2}(y_n - a)^2)}{\exp(-\frac{E_b}{2\sigma^2}(y_n + a)^2)} \tag{2.10}$$

$$= -\frac{E_b}{2\sigma^2}(y_n - a)^2 - (-\frac{E_b}{2\sigma^2}(y_n + a)^2) \tag{2.11}$$

$$= 4a\,\frac{E_b}{2\sigma^2}y_n \tag{2.12}$$

$$= L_c\,y_n, \tag{2.13}$$

where $L_c = 4a\,\frac{E_b}{2\sigma^2}$ defines the channel reliability that depends on the instantaneous SNR and it varies due to fading variation of the channel. The extrinsic LLR L_e is fed back to the other constituent decoder, where it is used as *a priori* LLR of the bits in the next iteration.

2.1.3 EXIT Chart

EXIT Chart is first introduced by Stephan Ten Brink in [12]. It is used for visualizing the flow of extrinsic information exchange between the inner and outer decoders of a serially concatenated schemes or between the upper and lower decoders of parallel-concatenated schemes. EXIT Chart also visualizes the convergence behaviour of iterative decoding algorithms; thereby we can predict the convergence property, the algorithms based on which we can design good codes as well. Specifically, we can achieve infinitesimally low BER if the EXIT curves reach the [1.0,1.0] mutual information (MI) point, while keeping the convergence tunnel open.

Fig. 2.4 illustrates an example of EXIT chart; it shows EXIT curves of the decoders of convolutional codes with memory-1 and memory-2 that are used in this thesis. Let $\mathbf{b}$ denotes the sequence of information bits and $\mathbf{X}$ be the output of convolutional codes with the generator polynomials of $G = [3, 2]_8$ and $G = [7, 5]_8$ for the memory-1 or the memory-2 codes, respectively. At the receiver side, for the decoder, we generate *a priori* LLR L_a as

$$L_a = \rho x + \eta, \tag{2.14}$$

where $x \in \{+1, -1\}$ denotes the binary phase shift keyed (BPSK) sequence of $\mathbf{X}$, η denotes zero mean AWGN, and $\rho = \sigma^2/2$ with σ^2 denoting the variance of the noise. It is necessary to assume that a large enough interleaver is employed to assure statistical independence and Gaussian distribution of L_a.

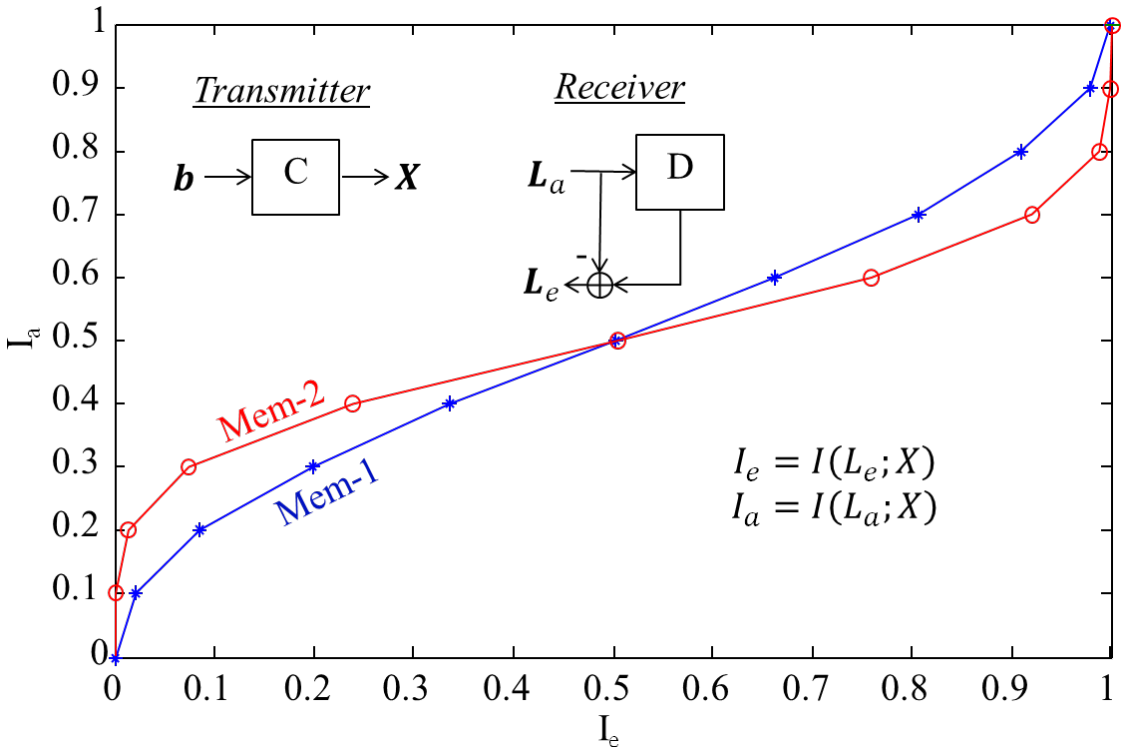

Figure 2.4. EXIT Chart of Convolutional Codes Decoder

The information transfer function T is measured as

$$I(L_e; \mathbf{X}) = T(I(L_a; \mathbf{X})), \tag{2.15}$$

where the input, $I(L_a; \mathbf{X})$, denotes the MI between the transmitted encoded bit sequence $\mathbf{X}$ and the *a priori* LLR, and the output, $I(L_e; \mathbf{X})$, denotes the MI between the $\mathbf{X}$ and the extrinsic LLR. We use I_a to denote *a priori* MI $I(L_a; \mathbf{X})$ and I_e to denote extrinsic MI $I(L_e; \mathbf{X})$. It is found that MI is a function of the variation of LLR. Given $0 \leq I_a \leq 1$, we can convert the MI value to its corresponding LLR variation σ by an approximation given by [13]

$$\sigma(I) \approx (-\frac{1}{H_1} \log_2(1 - I^{\frac{1}{H_3}}))^{\frac{1}{2H_2}}, \tag{2.16}$$

where $H_1 = 0.3073$, $H_2 = 0.8935$, and $H_3 = 1.1064$, and I = I_a or I_e, depending on LLR = L_a or LLR = L_e, respectively. It should be noted that for inner decoder, the channel SNR is also an input parameter.

2.2 Automatic Repeat reQuest

FEC error control systems in principle is assumed in simplex channels, i.e. in the channels where the information flow is only towards one direction. If the channel is duplex, we can also allow the acknowledge information to be transmitted in back to the transmitter via feedback channel. In this scheme, the transmitted information data is first encoded by CRC for error detection. The receiver sends either acknowledgment (ACK) or negative ACK (NACK) signal via the feedback channel to indicate whether the transmitted data packet has been correctly received or not, respectively. In ARQ system design, it is commonly assumed that feedback channel is error-free, because the information to be transmitted via the feedback channel is only one bit, i.e. ACK and NACK.

Based on the retransmission strategies, there are three basic protocols of ARQ schemes: stop-and-wait, go-back-N, and selective-repeat. Stop-and-wait is the simplest protocol. After transmission, the transmitter waits for a feedback from the receiver. If an ACK is received, the next message is transmitted; if a NACK is received, the message is retransmitted. Packet retransmission continue until an ACK is received. This scheme is inefficient since the channel stays idle between transmissions.

With the go-back-N protocol, groups of N packets are transmitted, and each group requires only one feedback, i.e. ACK or NACK. If one or more packets in a group is/are received incorrectly, the last *N* packets are retransmitted. This scheme eliminates the idle time between transmissions for every message, which is a negative point of the stop-and-wait scheme. Obviously, go-back-N protocol is more efficient than stop-and-wait protocol.

Selective-repeat protocol further improve the efficiency of go-back-N protocol by retransmitting only packets that have not been received correctly. However, the go-back-N protocol requires large buffer at the transmitter and the receiver, and the selective-repeat protocol requires, in theory, infinite size of buffer.

The performance of an ARQ system can be measured by its throughput efficiency. The throughput of stop-and-wait, go-back-N, and selective-repeat protocols are given by [14]:

$$\eta_{sw} = \frac{K(1-P_B)}{L_B + R_s\,\Delta T}, \tag{2.17}$$

$$\eta_{gn} = \frac{K(1-P_B)}{L_B + R_s\,\Delta T P_B}, \tag{2.18}$$

and

$$\eta_{sr} = \frac{K}{L_B}(1-P_B), \tag{2.19}$$

respectively, where K is the number of bits per block, L_B is the block length in symbols, P_B is the block error probability, R_s is the signalling speed over channel in symbols/seconds, and ΔT is the overall round-trip delay.

2.3 Hybrid ARQ

The term HARQ is used to describe combine used of FEC+ARQ. If the received packet is found to contain error(s) in its information part after the FEC decoding is performed, the receiver sends a retransmission request to the transmitter. FEC is used to correct the errors, however, if the number of errors exceeds its correction capability, which is found by error detection code such as CRC after the FEC decoding, a retransmission is requested. This makes the decoder structure simple while improving the reliability, and hence enhance the throughput. Therefore, HARQ can eliminate the drawbacks of

both/either FEC and/or ARQ schemes/alone.

Based on the chronicle of research on HARQ, the HARQ can be classified into two types [15]. For type-I HARQ, retransmitted packet is FEC-decoded, and the packet is discarded if errors are detected after the FEC-decoding. Hence, the receiver combines the current packet with none of the previously received packets in decoding. For type-II HARQ, all transmitted packets associated with the same information data block are jointly decoded instead of discarding the packet of which decoding is failed, thus reducing the probability of decoding error. The type-II HARQ can be further classified into two categories: the first kind is often called *Chase combining* (CC), where all retransmissions are identical, including the parity part.

The other is often called incremental redundancy (IR), where the rate compatible punctured code is used; for the first transmission, high rate FEC is designed by utilizing the optimal puncturing pattern from a relatively low rate mother code, and used after the CRC encoding for error detection; for the first retransmission and later on, the punctured parts, each having the same length, are transmitted to provide receiver with additional redundancy. Hence, the more the retransmissions are performed, the lower the effective code rate. The rate-compatible property of the low-rate code provides even more powerful error correction capability than CC, and enables reconstruction of the message uniquely from the parity block.

In the framework of Turbo HARQ, the CC is typically used with CBD, whereas the IR is typically used with packet CAD, as described in the following Sections.

2.4 Packet Combining in Turbo HARQ

2.4.1 Combining Before Decoding (CBD)

In ARQ systems over multipath fading channels, transmissions experience difference channel realizations, transmission-by-transmission. Obviously, the packets of the second and following transmissions can be independently equalized and decoded to obtain the desired information bits. However, retransmitted packets could be jointly equalized and decoded since they contain common information part. To enable the joint equalization, the algorithm of the standard equalization has to be modified so that signal samples, received in each retransmission phase, are combined by the equalizer. This concept of CBD is referred to as IEQ in [7] or as CBD-IEQ in this thesis.

The IEQ's turbo equalizer has inputs: received signals $\mathbf{y}_n^{(k)}$ and *a priori* information

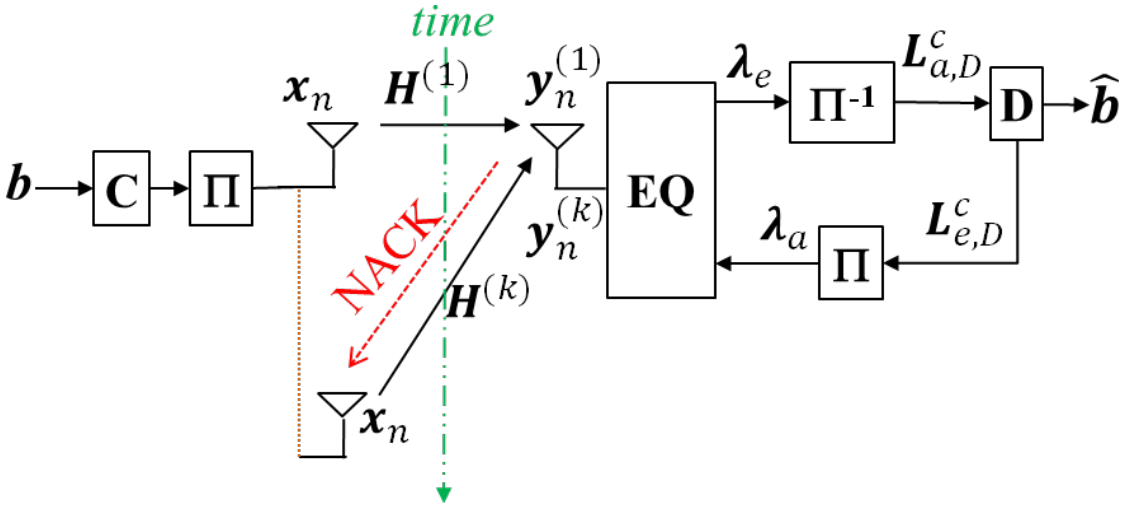

Figure 2.5. CBD-IEQ Turbo HARQ Systems

λ_a, as illustrated in Fig. 2.5. λ_a is obtained from the interleaved extrinsic information output from the channel decoder in the form of extrinsic LLR, $L^c_{e,D}$, of the coded bits. Hence, the λ_a represents the reliability of the transmitted signals $\mathbf{x}_n$.

In the transmitter side, the signal vector $\mathbf{x}_n$ is formed by first encoding the information bits vector $\mathbf{b}$ with the encoder C, followed by interleaving $\mathbf{b}$ with an interleaver Π, and finally being transmitted over the multipath channel. This structure forms SCC where the channel is the inner encoder because the multipath channel can be modelled by a tapped delay time which is equivalent to a convolutional code defined over the *Complex Field*. The transmitter stores $\mathbf{x}_n$ in a buffer for further retransmissions when it receives an NACK, corresponding $\mathbf{x}_n$, from the receiver. At the receiver, the received signal $\mathbf{y}_n^{(1)}$ of the first transmission can be expressed as

$$\mathbf{y}_n^{(1)} = \mathbf{H}^{(1)}\mathbf{x}_n + \mathbf{v}_n^{(1)} \in \mathbb{C}^{N\times 1}, \tag{2.20}$$

where $\mathbf{v}_n^{(1)}$ denotes a zero mean complex AWGN vector with variance σ^2, corresponding to the channel SNR. Signal detection and equalization is then performed by an equalizer EQ. Afterwards, the extrinsic output of the EQ in the form of LLR is deinterleaved by Π^{-1}, giving an *a priori* information, $L^c_{a,D}$, to the channel decoder D. Horizontal iteration(s) (*HI*s) is(are) performed between the EQ and the D according to the turbo principle. If error/errors is/are detected by CRC after performing enough times of *HI*s, the receiver sends a NACK, and stores the $\mathbf{y}_n^{(1)}$ and the current channel state

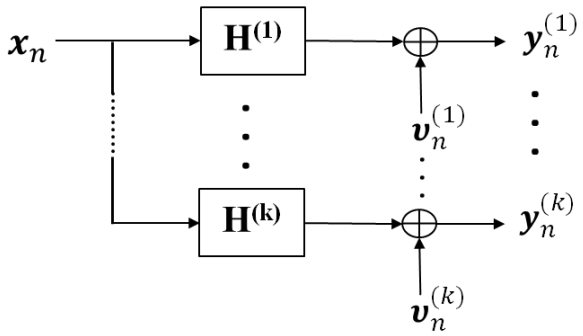

Figure 2.6. SIMO Channel Model

information $\mathbf{H}^{(1)}$ for signal combining to be performed in the following transmission phases.

For the $(k-1)$-th retransmission phase, the received signal can be expressed as

$$\mathbf{y}_n^{(k)} = \mathbf{H}^{(k)}\mathbf{x}_n + \nu_n^{(k)} \in \mathbb{C}^{N\times 1}, \tag{2.21}$$

hence the channel is equivalent to SIMO system as illustrated in Fig. 2.6. It is worth noticing that the CBD-IEQ technique does not optimally exploit the advantage of the time diversity gain because turbo equalization is performed for the coded sequence having the same bit pattern, as shown in Ref. [9]. Reference [9] then proposes an alternative of CBD which improves the turbo-diversity scheme to CBD-IEQ by exploiting different interleaver in every retransmission to reduce the Euclidean distance dispersion, referred to as TDT in [9] or CBD-TDT in this thesis.

The block diagram of the CBD-TDT is shown in Fig. 2.7. At the transmitter, the same codeword is interleaved by Π_n in every k-th transmission, yielding transmitted signal $x_n^{(k)}$. At the receiver, turbo equalizations of received signals $\mathbf{y}_n^{(k)}, k = (1, 2, ..., K)$, are performed independently and hence the packet combining can not be performed with the equalization process as in IEQ. Instead, the packet combining is performed by accumulating all *a priori* information to the channel decoder, as

$$L_s^c = \sum_{i=1}^{k} L_{a,D}^{c(i)} \in \mathbb{C}^{N\times 1}. \tag{2.22}$$

The L_s^c is updated in the *HI* loop of every retransmission phase. Furthermore the same coded bits are fed back to the equalizers.

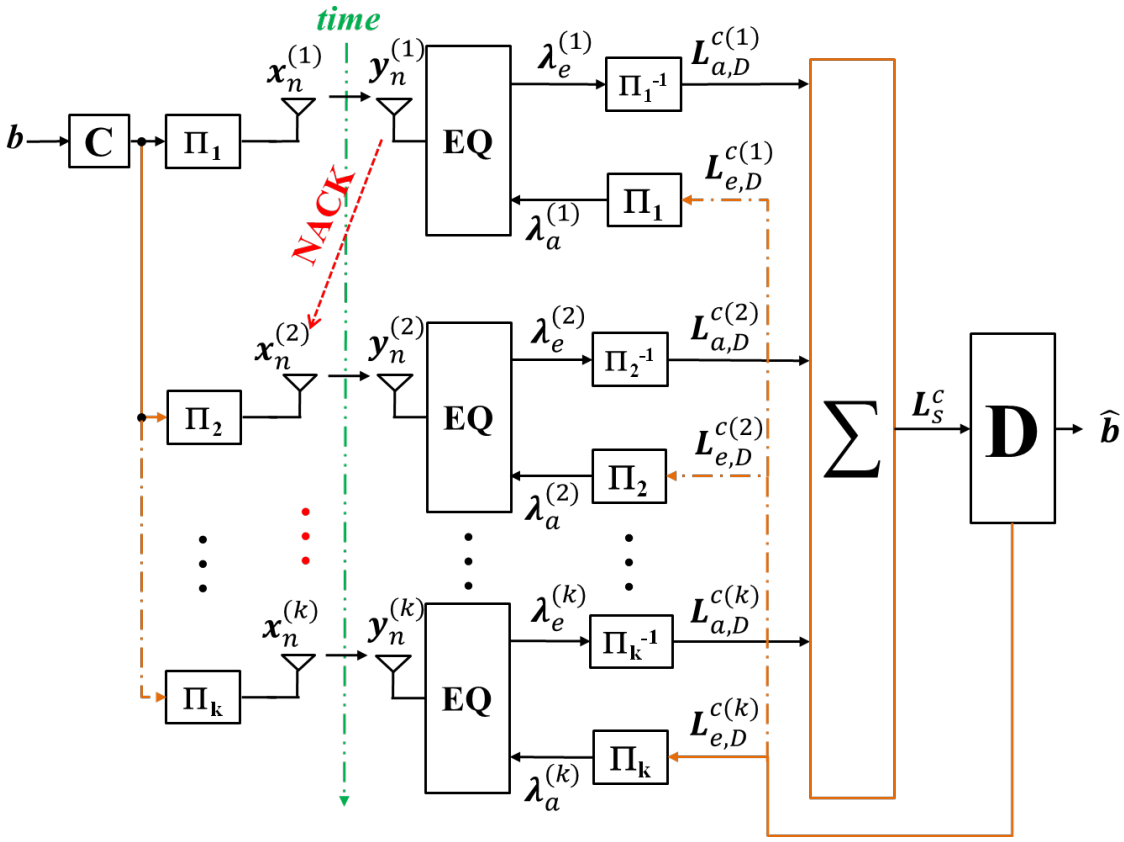

Figure 2.7. CBD-TDT Turbo HARQ Systems

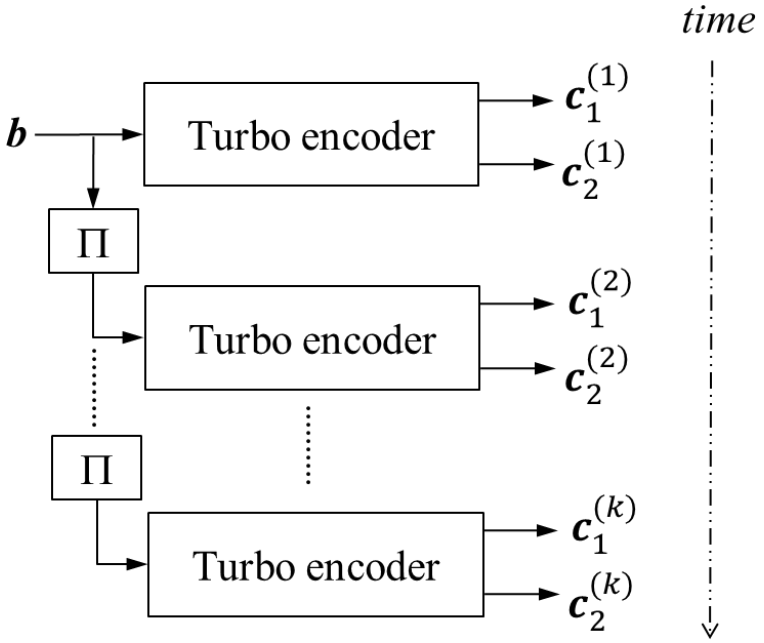

Figure 2.8. Conventional CAD Encoder, $K = 2$

2.4.2 Combining After Decoding (CAD)

CAD refers to the technique proposed in [3], where the HARQ system forms parallel concatenation of multiple turbo codes, which is corresponding to multiple transmissions of the same information. The encoder structure of this conventional CAD for one retransmission is shown in Fig. 2.8. The Turbo encoder follows the structure shown in Fig. 2.3. If NACK is received, the data sequence $\mathbf{b}$ is interleaved using interleaver Π, encoded by an identical Turbo encoder, and then retransmitted. The interleaver has different interleaving pattern, retransmission-by-retransmission, as in Turbo encoder. This is essential to improve the performance, because with this technique, larger spectrum thinning effect can be achieved, according to the increase in retransmission times.

At the receiver side, the packet-wise CAD is performed to exploit the soft information expressed in the form of *a priori* LLR of the uncoded (systematic) bits obtained in the last transmission provided for the decoding of the current transmission.

2.4.3 Outage Probability of CAD and CBD

The instantaneous SNR is defined as $\gamma_i = \text{SNR}|h_i|^2$. The number of transmission of the same information is upper-bounded by K. Thus, the per-transmission capacity of

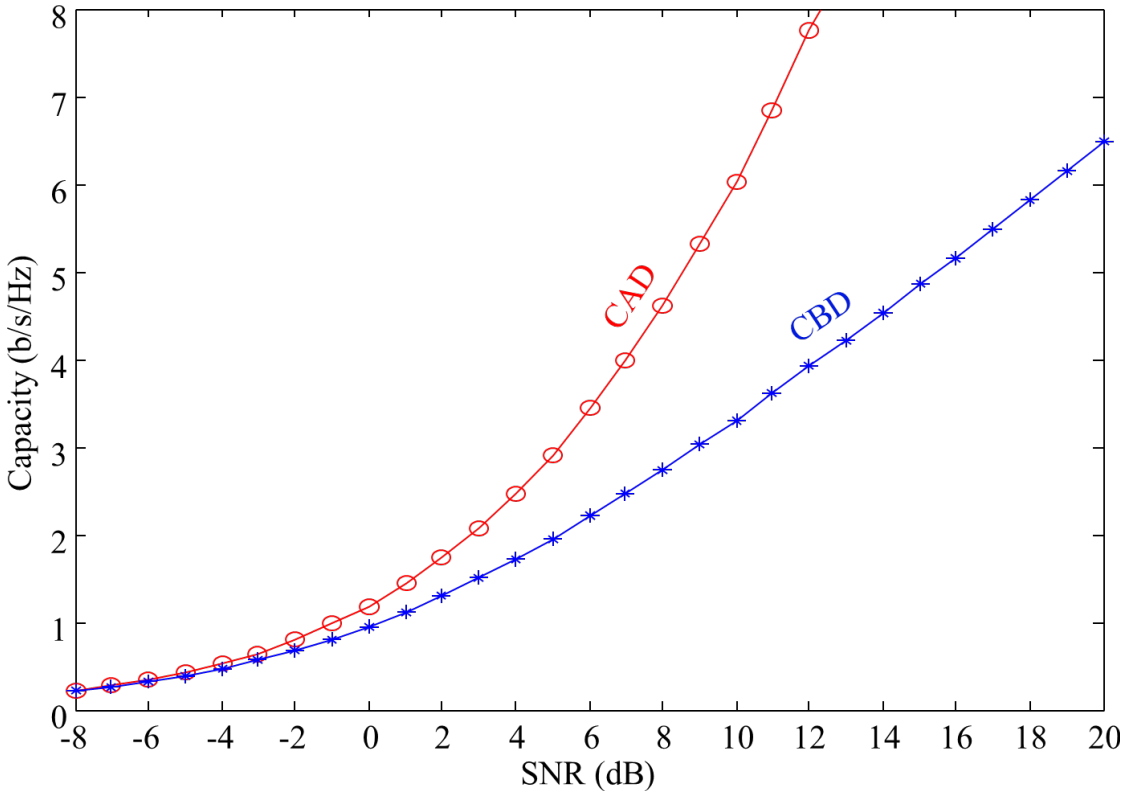

Figure 2.9. CAD and CBD capacities comparison for $K = 4$

CBD is given by

$$C_B = \log_2(1 + \sum_{i=1}^{K} \frac{\gamma_i}{K}), \tag{2.23}$$

whereas the per-transmission capacity of CAD is given by

$$C_A = \sum_{i=1}^{K} \log_2(1 + \frac{\gamma_i}{K}) = \log_2(\prod_{i=1}^{K}(1 + \frac{\gamma_i}{K})). \tag{2.24}$$

Since $\frac{\gamma_i}{K} \geq 0$, it is easy to prove that $C_A \geq C_B$. Examples of CAD and CBD capacity curves for $K = 4$ are shown in Fig. 2.9.

An Outage happens when the mutual information after K attempts of transmission is smaller than the required transmission rate, R. Therefore, the outage probability

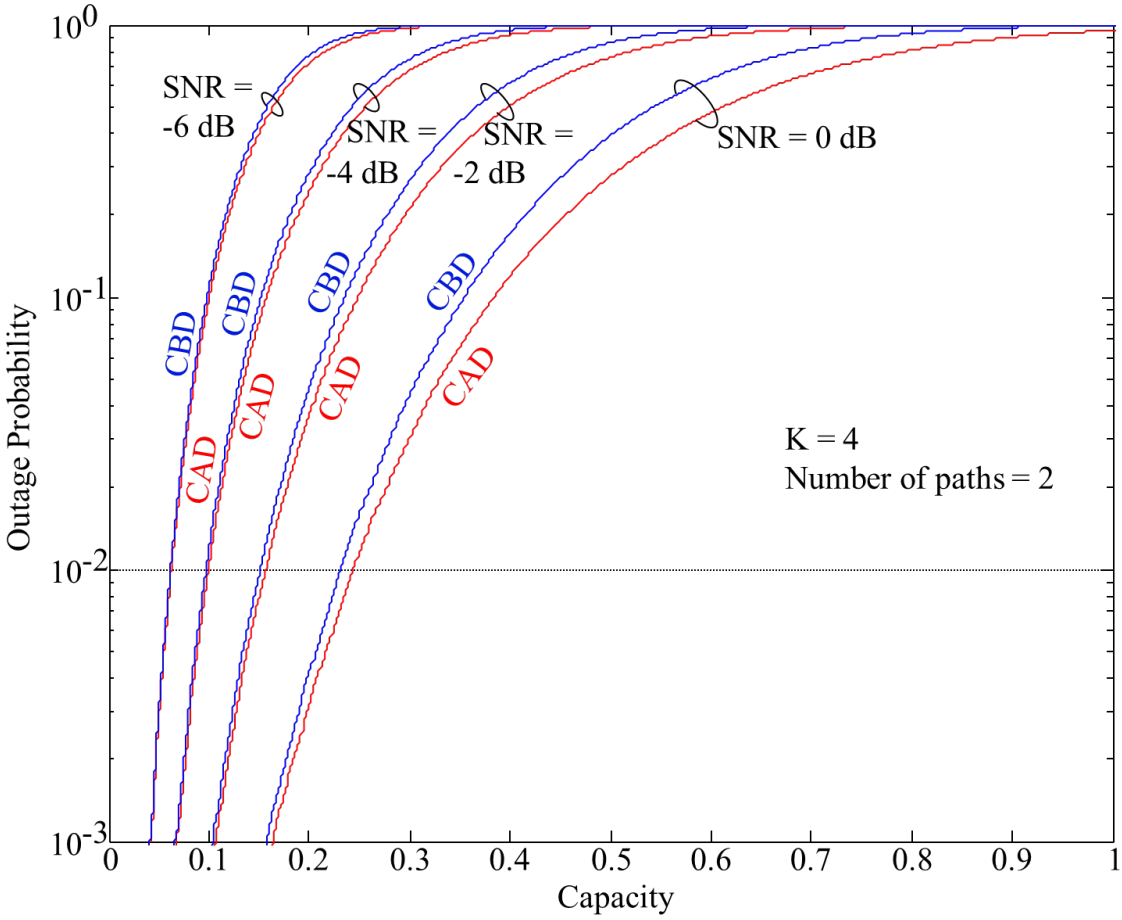

Figure 2.10. CCDF of the theoretical CAD and CBD capacities in multipath fading channels for $K = 4$

with CBD is given by

$$P_{out}^{B} = P_r \left[\log_2(1 + \sum_{i=1}^{K} \frac{\gamma_i}{K}) \leq R \right], \tag{2.25}$$

and the outage probability with CAD is given by

$$P_{out}^{A} = P_r \left[\sum_{i=1}^{K} \log_2(1 + \frac{\gamma_i}{K}) \leq R \right]. \tag{2.26}$$

Examples of CAD and CBD outage capacity curves for $K = 4$ obtained via simulations are shown in Fig. 2.10.

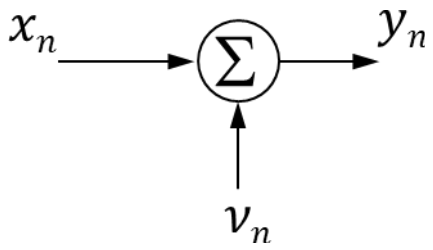

Figure 2.11. AWGN Channel Model

2.5 Channel Model

In this thesis, we consider two kinds of channels: AWGN and multipath fading channels, which are described in the following subsections.

2.5.1 AWGN

In AWGN channels, the transmitted signal suffers from a linear addition of a white noise having a constant spectral density and complex Gaussian-distributed. The block diagram is expressed in Fig. 2.11. The output y_n at discrete time index n is the sum of the input x_n and noise ν_n, where ν_n is independent and identically distributed (i.i.d.) zero-mean complex Gaussian distribution with variance σ^2. Then, for the notational convenience, all $y_n, n = \{1, 2, \cdots, N\}$, are sorted into a vector, as $\mathbf{y} = (y_1, y_2, \cdots, y_N)^T$, yielding the vectorized input-output relationship of the channel is given by

$$\mathbf{y} = \mathbf{x} + \mathbf{v}, \tag{2.27}$$

where $\mathbf{x} = (x_1, x_2, \cdots, x_N)^T$ and $\mathbf{v} = (\nu_1, \nu_2, \cdots \nu_N)^T$ are statistically independent.

2.5.2 Multipath Fading

In multipath fading channel, the path between the transmitter and receiver is subject to various obstacles and reflections. The received composite wave is composed of many component waves such as reflected, diffracted, and scattered waves, and direct wave from the transmitter. In this case, the path lengths of the direct, reflected, diffracted, and scattering waves are different, resulting in different arrival timing at the receiver, and each experiencing different attenuations and phase rotations. Consequently, the receiver receives a superposition consisting of several component waves having different

phases, amplitudes, and times of arrival.

Because of the dispersion due to multipath propagation, the transmitted signal experiences either flat or frequency selective fading. If the symbol period is much larger than the multipath time delay spread of the channel, or equivalently if the coherence bandwidth of the channel is much larger than the bandwidth of the signal, the received signal experiences flat fading. In this case, the impact of the arrival time dispersion of the component waves can be eventually ignored. Hence, all frequency components of the signal experience the same fading variation. Conversely, if the symbol period is smaller than the multipath time delay spread of the channel, or equivalently if the coherence bandwidth of the channel is less than the bandwidth of the signal, the received signal experiences selective fading.

Assuming block fading, where the channel complex envelope h is constant over one block, the received signal can be expressed as

$$\mathbf{y} = h\,\mathbf{x} + \mathbf{v} \in \mathbb{C}^{(N)\times 1}, \tag{2.28}$$

whereas in frequency selective fading case, the received signal can be expressed as

$$\mathbf{y} = \mathbf{H}\,\mathbf{x} + \mathbf{v} \in \mathbb{C}^{(N+L-1)\times 1}, \tag{2.29}$$

where L is the number of paths in the frequency selective fading channel. The channel matrix $\mathbf{H}$ has a Toeplitz structure, as

$$\mathbf{H} = \begin{bmatrix} h_0 & & & 0 \\ \vdots & h_0 & & \\ h_{L-1} & \vdots & \ddots & \\ & h_{L-1} & \vdots & h_0 \\ & & \ddots & \vdots \\ 0 & & & h_{L-1} \end{bmatrix} \in \mathbb{C}^{(N+L-1)\times N}, \tag{2.30}$$

In this thesis, we assumed that the magnitude of a signal that has passed through a channel varies randomly following Rayleigh distribution. The Rayleigh fading channel is modelled by sum-of-sinusoids simulators, introduced by Jakes in [16], known as Jakes' simulator or Jakes model. This channel model has been widely used in wireless mobile communication community [17]. However, as investigated in [17], the Jakes model

has a shortcoming that the rays experiencing the same Doppler frequency shift are correlated, resulting in a mismatch to the real natural phenomena. Therefore, we use the improved version of Jakes' model proposed in [17].

The simulator output complex envelope h is given by

$$h(t) = \upsilon_c(t) + j\,\upsilon_s(t), \tag{2.31}$$

where

$$\upsilon_c(t) = \frac{2}{\sqrt{\aleph}} \sum_{m=1}^{\mathcal{M}+1} a_m \cos(\omega_m t + \theta_m), \tag{2.32}$$

$$\upsilon_s(t) = \frac{2}{\sqrt{\aleph}} \sum_{m=1}^{\mathcal{M}+1} q_m \cos(\omega_m t + \theta_m), \tag{2.33}$$

$$a_m = \begin{cases} 2\cos(\beta_m), m = \{1, 2, \cdots, \mathcal{M}\} \\ \sqrt{2}\cos(\beta_{\mathcal{M}+1}), m = \mathcal{M}+1 \end{cases} \tag{2.34}$$

$$q_m = \begin{cases} 2\sin(\beta_m), m = \{1, 2, \cdots, \mathcal{M}\} \\ \sqrt{2}\sin(\beta_{\mathcal{M}+1}), m = \mathcal{M}+1 \end{cases} \tag{2.35}$$

$$\beta_m = \begin{cases} \frac{\pi m}{\mathcal{M}}, m = \{1, 2, \cdots, \mathcal{M}\} \\ \frac{\pi}{4}, m = \mathcal{M}+1 \end{cases} \tag{2.36}$$

$$\omega_m = \begin{cases} \omega_d \cos(\frac{2\pi m}{\aleph}), m = \{1, 2, \cdots, \mathcal{M}\} \\ \omega_d, m = \mathcal{M}+1 \end{cases} \tag{2.37}$$

$$\omega_d = 2\pi f_d, \tag{2.38}$$

$$\tag{2.39}$$

$\aleph = 4\mathcal{M}+2$ is the number of incoming waves, with $\mathcal{M}$ being an interim parameter, and θ_m is random variables uniformly distributed over $[-\pi, \pi)$ for all m. It should be noted here that h in (2.31) should apply to that in (2.28), as well as to $\{h_0, h_1, \cdots, h_{L-1}\}$ in (2.30).

2.6 Turbo Equalization

In block transmission systems, a transmission over multipath fading channel causes multiple copies of the transmitted blocks, each scaled independently by their fading complex envelope $h_l, 0 \leq l \leq L-1$, and arrives at the receiver at different timings

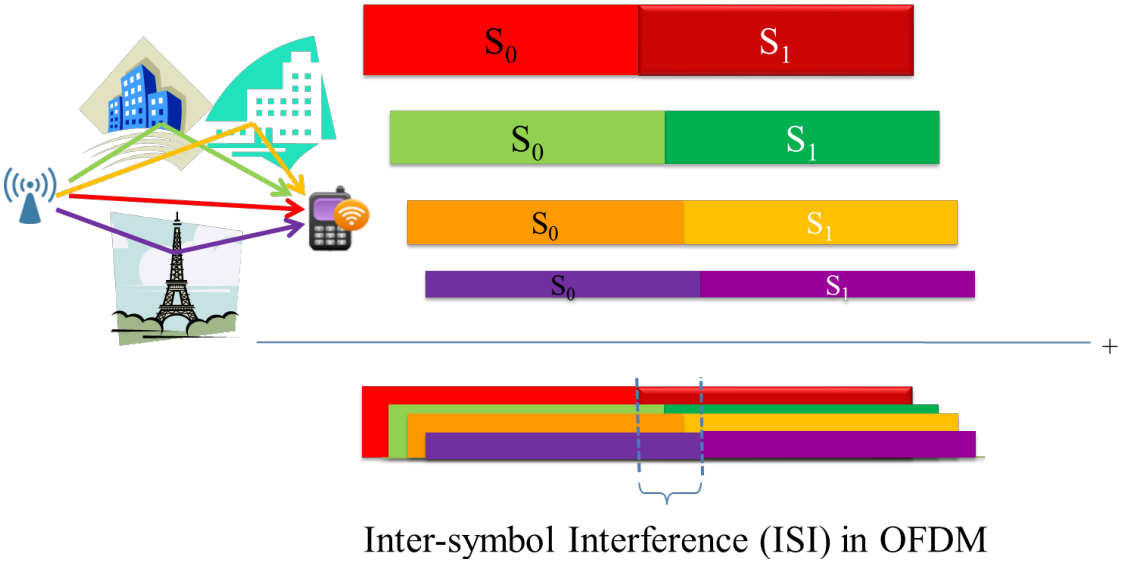

Figure 2.12. Multipath Fading Problem: Inter-symbol Interference

as described in the previous Subsection. This causes inter-symbol interference (ISI) within one block. Furthermore, the length of GI, placed between consecutive blocks, has to be greater than that of channel impulse response (CIR) to avoid the IBI; if the GI length is insufficient, single carrier signalling suffers from inter-block interference (IBI), and OFDM from ISI, as illustrated in Fig. 2.12. Those interference components cause serious distortion in the received signal. However, appending GI introduces redundancy and thereby degrades the bandwidth efficiency. Hence, the GI should be as short as possible. As a result, there exists the possibility that the CIR interval exceeds the duration of GI, resulting in severe IBI, caused in the consecutive blocks.

A solution to mitigating the harmful effects of IBI is to perform filtering at the receiver, called equalizer. FD-SC/MMSE is a core part of the HARQ systems over frequency selective fading channels, which is the core part of the investigations in this thesis. Subsection 2.6.1 only briefly touch upon the FD-SC/MMSE equalization technique because it is already well known and widely used in broadband single carrier wireless communication systems [18] with CP transmission, where CP is used as GI.

In Subsection 2.6.2, a novel technique, the CHATUE algorithm that can eliminate the necessity of the CP transmission is provided, however, the CHATUE algorithm derivation is for OFDM instead of single carrier signalling. This is because the research on CHATUE for OFDM systems, referred to as CHATUE-OFDM, has been financially supported by the project sponsors, SANYO Electric Co., Ltd and Kinki Mobile Radio

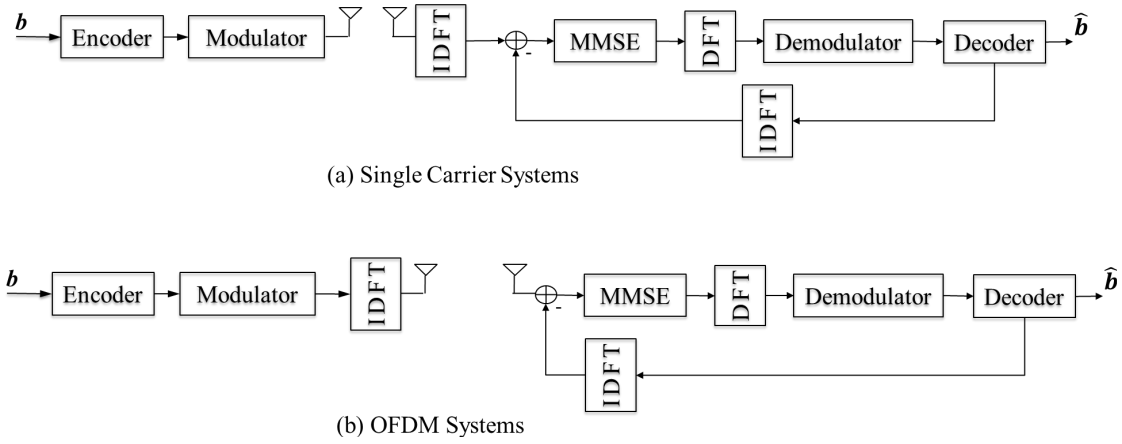

Figure 2.13. FD-SC/MMSE in Single Carrier and OFDM Systems

Center Inc.

2.6.1 FD-SC/MMSE Equalization in Single Carrier Systems

Several techniques have been proposed in the literatures to overcome the problem of ISI. A sub-optimal turbo equalization technique, FD-SC/MMSE [19], can achieve asymptotically optimal performance in single carrier block transmission with a sufficient CP length compared with the channel memory length, without requiring heavy computational burden. Furthermore, the FD-SC/MMSE algorithm can be modified into CHATUE algorithm so that the both ISI and IBI components can be cancelled without having to transmit CP, as proposed in [20]. Hence, significant improvement in bandwidth efficiency can be achieved by using the CHATUE algorithm, as shown in [20].

The single carrier FD-SC/MMSE algorithm that requires the CP transmission is applied to all Turbo HARQ systems evaluated in this thesis in multipath fading channels. Furthermore, the single-carrier FD-SC/MMSE [19] can easily be converted to OFDM by replacing the position of inverse DFT (IDFT), as shown in Fig. 2.13. Therefore, the CHATUE algorithm can be further applied to OFDM systems as described in the following subsections.

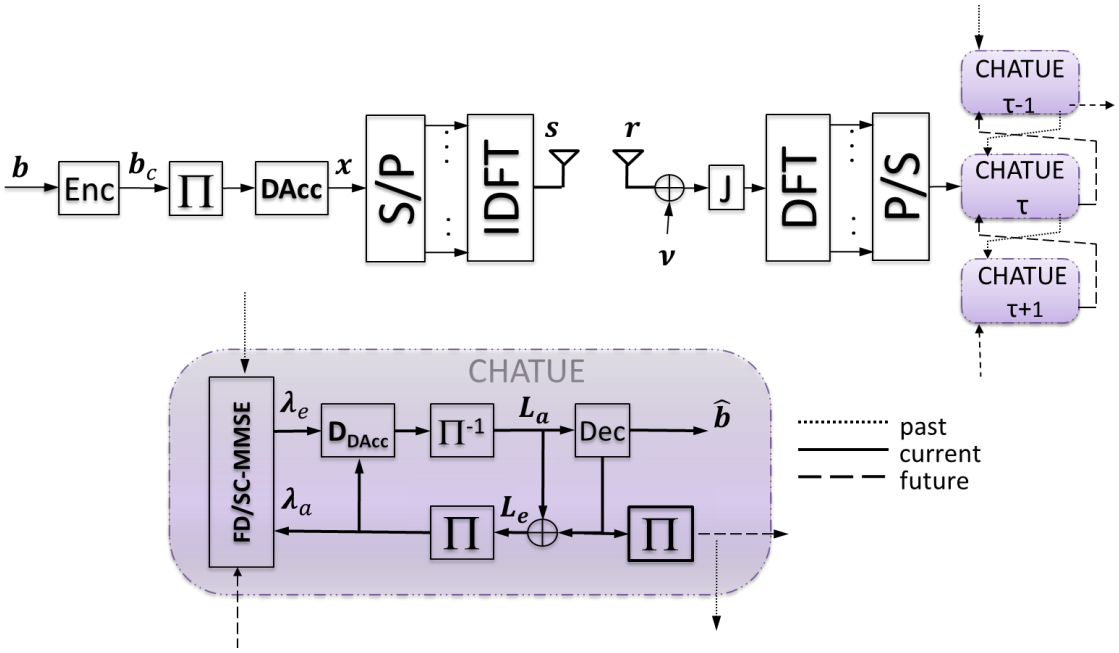

Figure 2.14. CHATUE OFDM Systems

2.6.2 CHATUE-OFDM

OFDM has been chosen for several wireless broadband standards such as IEEE 802.16 wireless metropolitan networks, IEEE 802.11a and HIPERLAN/2 wireless local area networks, terrestrial digital audio broadcasting (DAB-T), and terrestrial video broadcasting (DVB-T). Such services need to accommodate as many users as possible within the limited frequency bandwidth. Therefore, spectrally efficient broadband schemes have to be created, which can be satisfied by using the CHATUE algorithm. With CHATUE, turbo equalizers for several consecutive OFDM symbols exchange information about the interference to effectively suppress ISI, and inter-carrier interference (ICI).

The system model of the CHATUE-OFDM, considered in this thesis, is shown in Fig. 2.14. At the transmitter side, the information bit sequence $\mathbf{b}$ are encoded by the encoder Enc, of which results are made statistically independent by using bit interleaver Π, yielding bit-interleaved sequence $\mathbf{b}_c$. The sequence $\mathbf{b}_c$ is then doped-accumulated [21] by $DAcc$, yielding $\mathbf{x}$. In the OFDM system, we use IDFT to acquire the orthogonality of the signal in order to effectively utilize the frequency spectrum and enhance the robustness over multipath fading. Here $\mathcal{N}$-point IDFT transforms $\mathbf{x}$ into OFDM symbols into block sequence $\mathbf{s}$. The block $\mathbf{s}$ is transmitted over frequency-

selective quasi static block Rayleigh fading channel of which the channel matrix has a Toeplitz structure as shown in (2.30).

At the receiver side, we exploit the matrix $\mathbf{J}$ [22], expressed as

$$\mathbf{J} = \left[\begin{array}{c|c} \begin{array}{c} 0_{(\mathcal{N}-L+1)\times(L-1)} \\ \\ \mathbf{I}_{(L-1)} \end{array} & \mathbf{I}_{\mathcal{N}} \end{array}\right] \in \mathbb{C}^{\mathcal{N}\times(\mathcal{N}+L-1)}, \tag{2.40}$$

for non-CP-transmission scheme, to obtain the $\mathcal{N} \times \mathcal{N}$ circulant matrix structure of the channel as in the CP-transmission schemes. The current received signal, suffering from AWGN, can be written as

$$\mathbf{r}_t = \mathbf{J}\mathbf{H}'_{t-1}\mathbf{s}'_{t-1} + \mathbf{J}\mathbf{H}_t\mathbf{s}_t + \mathbf{J}\mathbf{H}''_{t+1}\mathbf{s}''_{t+1} + \mathbf{J}\mathbf{v} \in \mathbb{C}^{\mathcal{N}\times 1} \tag{2.41}$$

after the $\mathbf{J}$ matrix multiplication, where $\mathbf{s}'_{t-1}$, $\mathbf{s}_t$, and $\mathbf{s}''_{t+1}$ denote $\mathcal{N} \times 1$ vectors of the current, the past, and the future OFDM symbols, respectively. DFT is applied to $\mathbf{s}$, in order to retrieve the frequency domain representation of the signal, denoted by $\mathbf{y}$.

Since the CHATUE is not the focus issue of this thesis, we leave the details in the Appendices of this thesis. The derivation of the CHATUE-OFDM algorithm is provided in Appendix A. Furthermore, results of performance simulations by using parameters given in Table C.1. shown in Appendix C.1. BER performance improvement achieved by CHATUE-OFDM over OFDM with CP transmission, both having the same spectral efficiency, is demonstrated in the figures in Appendix C.1.

2.6.3 CHATUE for Multiuser SIMO OFDM

It is well known that multiple input multiple output (MIMO) techniques offer significant increases in data throughput without requiring additional bandwidth or transmission power. It is made possible in the the form of spatial multiplexing or diversity gains. Hence, a combination of MIMO and OFDM appears to be one of the most efficient techniques for next generation broadband wireless communication systems.

We apply the CHATUE algorithm for the multiuser single input multiple output OFDM (MU-SIMO-OFDM) systems. It is quite easy to modify the algorithm such that it can well suited to MIMO-OFDM. The system model of MU-SIMO-OFDM is shown in Fig. 2.15.

We consider a MU-SIMO-OFDM system with K_T users, K_R receive antennas, and

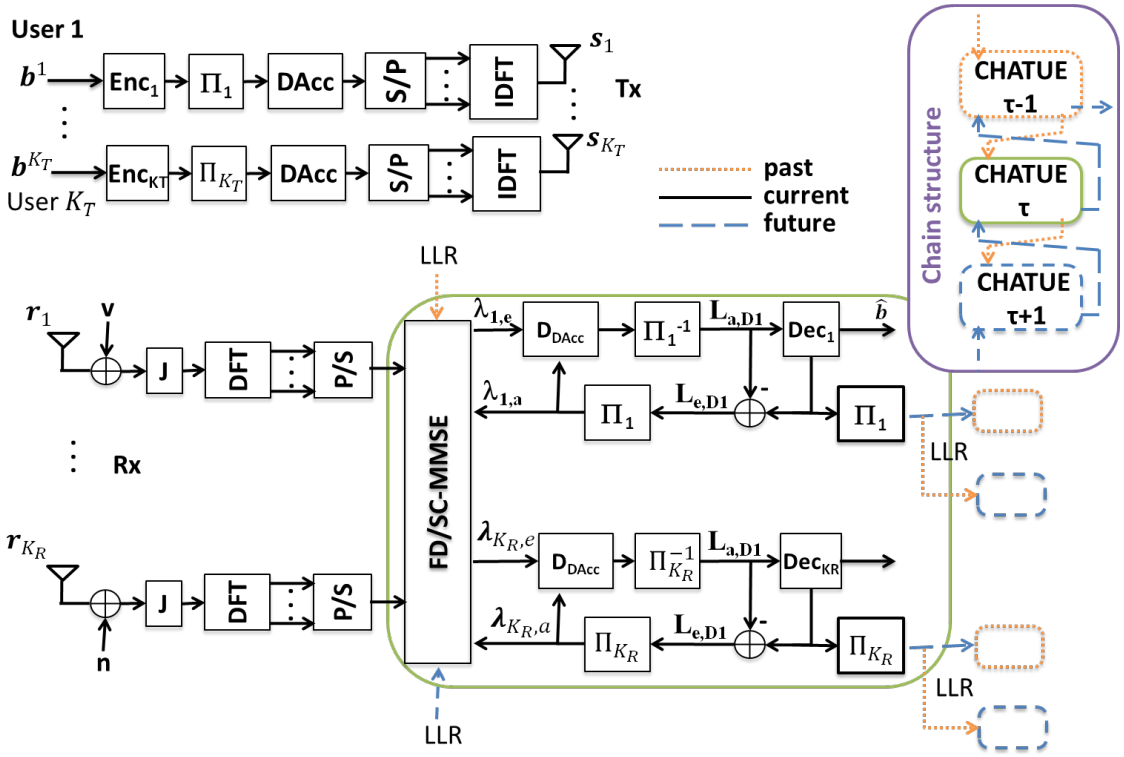

Figure 2.15. Multiuser CHATUE OFDM Systems

$\mathcal{N}$ subcarriers. The channel is assumed to have L propagation paths, each separated by the symbol duration T. At each transmitter, the information bits $\mathbf{b}^{\rho}$ are encoded into coded bit sequence $\mathbf{b}_c$, interleaved by a random interleaver Π, and doped-accumulated yielding the sequence $\mathbf{x}^{\rho}$, where $\rho = \{1, ..., K_T\}$ is the user index. By applying $\mathcal{N}$-point IDFT, $\mathbf{x}^{\rho}$ is further transformed into an OFDM symbol $\{s_{t,n}^{\rho}\}_{n=0}^{\mathcal{N}-1}$, where n and t denote the OFDM subcarrier and symbol indexes, respectively. The transmitted block of sample sequence in the time domain then becomes

$$\mathbf{s}_t^{\rho} = \{s_{t,n}^{\rho}\}_{n=0}^{\mathcal{N}-1} \in \mathbb{C}^{\mathcal{N}\times 1}. \tag{2.42}$$

The block $\mathbf{s}_t^{\rho}$ is transmitted over frequency-selective block quasi-static Rayleigh fading channel. Let the block-wise channel matrix at the timing index t be denoted by

$$\mathbf{H}_t = \{\mathbf{H}_t^{\zeta,\rho}\} = \begin{bmatrix} \mathbf{H}_t^{1,1} & \mathbf{H}_t^{1,2} & \dots & \mathbf{H}_t^{1,K_T} \\ \mathbf{H}_t^{2,1} & \mathbf{H}_t^{2,2} & \dots & \mathbf{H}_t^{2,K_T} \\ \vdots & \vdots & \ddots & \vdots \\ \mathbf{H}_t^{K_R,1} & \mathbf{H}_t^{K_R,2} & \dots & \mathbf{H}_t^{K_R,K_T} \end{bmatrix}_t \in \mathbb{C}^{(\mathcal{N}+L-1)K_R\times\mathcal{N}K_T}, \tag{2.43}$$
$$\zeta = \{1, 2, ..., K_R\},$$
$$\rho = \{1, 2, ..., K_T\},$$

where the $(\mathcal{N} + L - 1) \times \mathcal{N}$ sub-matrix $\mathbf{H}_t^{\zeta,\rho}$ has a Toeplitz structure, as

$$\mathbf{H}_t^{\zeta,\rho} = \begin{bmatrix} h_0^{\zeta,\rho} & & & 0 \\ \vdots & h_0^{\zeta,\rho} & & \\ h_{L-1}^{\zeta,\rho} & \vdots & \ddots & \\ & h_{L-1}^{\zeta,\rho} & \vdots & h_0^{\zeta,\rho} \\ & & \ddots & \vdots \\ 0 & & & h_{L-1}^{\zeta,\rho} \end{bmatrix}_t \in \mathbb{C}^{(\mathcal{N}+L-1)\times\mathcal{N}}, \tag{2.44}$$
$$\zeta = \{1, 2, ..., K_R\},$$
$$\rho = \{1, 2, ..., K_T\},$$

We exploit a matrix $\mathbf{J} = \mathbf{I}_{K_R} \otimes \mathbf{J}_M$, where $\mathbf{J}_M$ is given by (2.40). The received

composite signal can then be expressed as

$$\mathbf{r}_t = \mathbf{J}\mathbf{H}'_{t-1}\mathbf{s}'_{t-1} + \mathbf{J}\mathbf{H}_t\mathbf{s}_t + \mathbf{J}\mathbf{H}''_{t+1}\mathbf{s}''_{t+1} + \mathbf{J}\mathbf{v} \in \mathbb{C}^{\mathcal{N}K_R \times 1} \tag{2.45}$$

with

$$\mathbf{s}_t = \left[\mathbf{s}_t^1, \mathbf{s}_t^2, \cdots, \mathbf{s}_t^{K_T}\right]^T, \tag{2.46}$$

$$\mathbf{s}'_t = \left[\mathbf{s}'^{\,1}_{\,t}, \mathbf{s}'^{\,2}_{\,t}, \cdots, \mathbf{s}'^{\,K_T}_{\,t}\right]^T, \tag{2.47}$$

$$\mathbf{s}''_t = \left[\mathbf{s}''^{\,1}_{\,t}, \mathbf{s}''^{\,2}_{\,t}, \cdots, \mathbf{s}''^{\,K_T}_{\,t}\right]^T, \tag{2.48}$$

where $\mathbf{n}$ represents AWGN $K_R(\mathcal{N}+L-1)\times 1$ matrix. The sub-matrices of the channel matrices $\mathbf{H}'_{t-1}$ and $\mathbf{H}''_{t+1}$ represent interference from the past and the future symbols, respectively, both of which having the same matrix structure as that in (2.44), as $\mathbf{H}'_{t-1} = \{\mathbf{H}'^{\,\zeta,\rho}_{\,t-1}\}$ and $\mathbf{H}''_{t+1} = \{\mathbf{H}''^{\,\zeta,\rho}_{\,t+1}\}$, are given by

$$\mathbf{H}'^{\,\zeta,\rho}_{\,t-1} = \begin{bmatrix} & h_{L-1}^{\zeta,\rho} & \cdots & h_1^{\zeta,\rho} \\ & & \ddots & \vdots \\ & & & h_{L-1}^{\zeta,\rho} \\ 0 & & & \end{bmatrix}_{t-1} \in \mathbb{C}^{(\mathcal{N}+L-1)\times\mathcal{N}}, \tag{2.49}$$

and

$$\mathbf{H}''^{\,\zeta,\rho}_{\,t+1} = \begin{bmatrix} & & & 0 \\ & & & \\ h_0^{\zeta,\rho} & & & \\ \vdots & \ddots & & \\ h_{L-2}^{\zeta,\rho} & \cdots & h_0^{\zeta,\rho} & \end{bmatrix}_{t+1} \in \mathbb{C}^{(\mathcal{N}+L-1)\times\mathcal{N}}, \tag{2.50}$$

respectively. The received signal can then be transformed into frequency domain by DFT as

$$\begin{aligned} \mathbf{y}_t &= \mathbf{F}\mathbf{J}\mathbf{H}'_{t-1}\mathbf{s}'_{t-1} + \mathbf{F}\mathbf{J}\mathbf{H}_t\mathbf{s}_t + \mathbf{F}\mathbf{J}\mathbf{H}''_{t+1}\mathbf{s}''_{t+1} + \mathbf{F}\mathbf{J}\mathbf{v} \\ &= \mathbf{F}\mathbf{J}\mathbf{H}'_{t-1}\mathbf{F}^H\mathbf{x}'_{t-1} + \mathbf{F}\mathbf{J}\mathbf{H}_t\mathbf{F}^H\mathbf{x}_t + \mathbf{F}\mathbf{J}\mathbf{H}''_{t+1}\mathbf{F}^H\mathbf{x}''_{t+1} + \mathbf{F}\mathbf{J}\mathbf{v} \in \mathbb{C}^{\mathcal{N}K_R\times 1}, \end{aligned} \tag{2.51}$$

where $\mathbf{F}$ is given by $\mathbf{F} = \mathbf{I}_{K_R} \otimes \mathbf{F}_{\mathcal{N}} \in \mathbb{C}^{\mathcal{N}K_R\times\mathcal{N}K_R}$.

It is well known that the complexity of the FD-SC/MMSE equalization is independent of the number of the propagation paths. However, the computational complexity of the block-wise processing is still large depending on the structure of the covariance matrices of the interference components, when FD SC/MMSE is applied to the CHATUE algorithm. Several approximation techniques are applied in the following, depending on the structure of the interference covariance matrices in order to further reduce the complexity.

We propose a technique for reducing the complexity of the matrix inversion $\mathbf{\Sigma}^{-1}$ presented in (B.6) in Appendix B. The matrix $\mathbf{\Sigma}$, defined by (B.4) also in Appendix B, can be divided into three parts, matrices $\mathbf{A}$, $\mathbf{B}$, and $\mathbf{C}$, where $\mathbf{A}$ stands for the covariance matrix of the residual interference in the current symbol, $\mathbf{B}$ for the covariance matrix of residual interference from the past and future components, and $\mathbf{C}$ for the noise covariance matrix. $\mathbf{J}$ matrix is utilized to convert the block-Toeplitz channel matrix $\mathbf{H}_t$ into a circulant-block matrix, which can further be converted into a diagonal block matrix in the frequency domain by exploiting DFT. Hence, as shown in Fig.2.16, the frequency-domain covariance matrix of the residual vector $(\mathbf{x}_t - \hat{\mathbf{x}}_t)$ in $\mathbf{A}$ can be approximated by a diagonal block matrix $\frac{1}{\mathcal{N}} tr(\Lambda)\mathbf{I}_{\mathcal{N}}$ [23].

The submatrices $\mathbf{B_{11}}$, $\mathbf{B_{12}}$, $\mathbf{B_{21}}$ and $\mathbf{B_{22}}$ in $\mathbf{B}$ contain information of the interference from the past and future symbols, and as indicated by the density in Fig. 2.16, each submatrix has dense part only at the top-left and bottom-right corners of the matrix. Therefore, to reduce complexity, we apply the following approximation to those matrices in the corners, as

$$\mathbf{B}_{\zeta\rho} \approx \mathbf{B}'_{\zeta\rho} = diag_M(\mathbf{B}_{\zeta\rho}), \tag{2.52}$$

where $diag_M(\mathbf{X})$ is the operator that extracts only M diagonal elements from the top-left and bottom-right corner parts of the argument matrix $\mathbf{X}$. Since $\mathbf{B}_{\zeta\rho}$ is a diagonal elements, it is also reasonable to use the approximation :

$$\mathbf{F}_{\mathcal{N}}\mathbf{B}'_{\zeta\rho}\mathbf{F}^H_{\mathcal{N}} = \frac{1}{\mathcal{N}} tr(\mathbf{B}'_{\zeta\rho})I_{\mathcal{N}}, \tag{2.53}$$

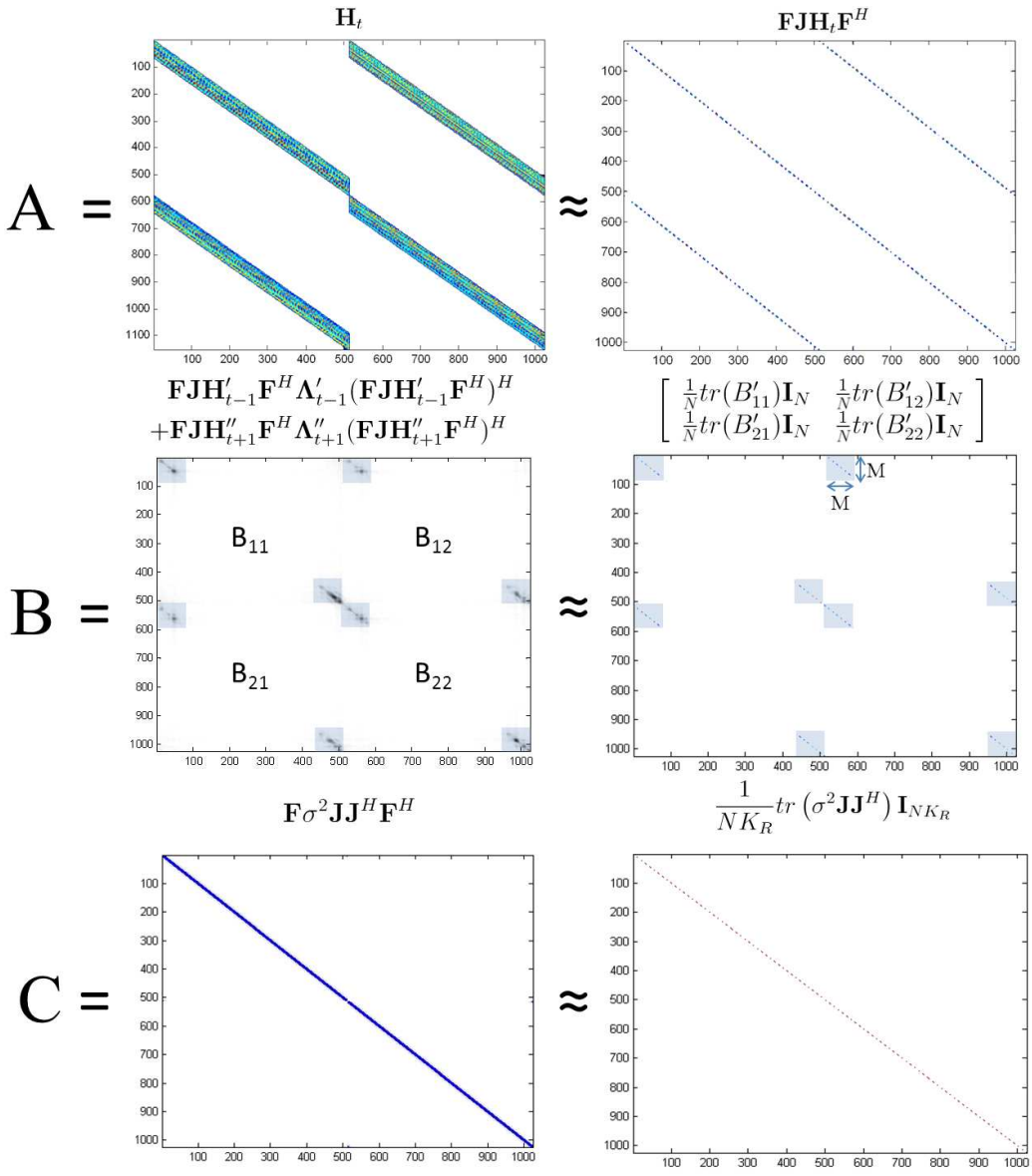

Figure 2.16. Approximations of Σ at *a priori* mutual information of past and future = 0.5

with which

$$\mathbf{F}\begin{bmatrix} \mathbf{B}'_{11} & \dots & \mathbf{B}'_{1K_T} \\ \mathbf{B}'_{21} & \dots & \mathbf{B}'_{2K_T} \\ \vdots & \ddots & \vdots \\ \mathbf{B}'_{K_R1} & \dots & \mathbf{B}'_{K_RK_T} \end{bmatrix}\mathbf{F}^H = \begin{bmatrix} \frac{1}{\mathcal{N}}tr(\mathbf{B}'_{11})I_{\mathcal{N}} & \dots & \frac{1}{\mathcal{N}}tr(\mathbf{B}'_{1K_T})I_{\mathcal{N}} \\ \frac{1}{\mathcal{N}}tr(\mathbf{B}'_{21})I_{\mathcal{N}} & \dots & \frac{1}{\mathcal{N}}tr(\mathbf{B}'_{2K_T})I_{\mathcal{N}} \\ \vdots & \ddots & \vdots \\ \frac{1}{\mathcal{N}}tr(\mathbf{B}'_{K_R1})I_{\mathcal{N}} & \dots & \frac{1}{\mathcal{N}}tr(\mathbf{B}'_{K_RK_T})I_{\mathcal{N}} \end{bmatrix} \in \mathbb{C}^{\mathcal{N}K_R\times\mathcal{N}K_R} \tag{2.54}$$

Hence, it is found that as shown in Fig.2.16, with the approximation technique presented above, the frequency domain representation of the covariance matrix of the residual interference from the past and future symbols becomes also diagonal block matrix, given by (2.54).

The matrix $\mathbf{C}$ is already diagonal matrix, and hence we can use also the approximation,

$$\mathbf{F}\sigma^2\mathbf{J}\mathbf{J}^H\mathbf{F}^H \approx \frac{1}{\mathcal{N}K_R}tr(\sigma^2\mathbf{J}\mathbf{J}^H)\mathbf{I}_{\mathcal{N}K_R}, \tag{2.55}$$

as shown in the same figure. Now that we have approximated $\mathbf{\Sigma}$ having two diagonal block and one diagonal matrices, $\mathbf{\Sigma}^{-1}$ can easily be calculated as in the original CHATUE algorithm.

The detailed derivation of the CHATUE-MU-SIMO-OFDM algorithm is provided in Appendix B. Furthermore, results of simulations by using parameters shown in Table C.1. in Appendix C.1, demonstrate the improvement of BER performance with CHATUE-OFDM over conventional OFDM system using CP transmission, both having the same spectral efficiency, as shown in Fig. C.7.

Chapter 3

Proposed Turbo HARQ: Doped-accumulator Assisted CAD

The transmitter of the turbo HARQ system proposed in this thesis is depicted in Fig. 3.1. The maximum times of transmission attempts is set at K ($K-1$ retransmissions). The bit stream $\mathbf{b}_0$ of the first transmission attempt is encoded by a rate R non-systematic non-recursive convolutional codes (NSNRCC) C_1. The output of C_1 is then interleaved by a random interleaver Π_1. The output of Π_1 is fed into doped accumulator $DAcc_1$ with a generator G = [3,2]$_8$. $DAcc_1$ introduces no redundancy and its decoder requires only moderate additional complexity. The doped-accumulated bits are modulated by BPSK. When the transmitter receives an ACK, the transmitter moves on to the next information frame transmission. If the transmitter receives a NACK, the transmitter retransmits the same information.

$\mathbf{b}_0$ is interleaved by different interleaver, retransmission-by-retransmission, yielding $\mathbf{b}_r = \Pi_r^v(\mathbf{b}_0)$,where $\Pi_r^v(\cdot)$ is the function performing vertical interleaving for the r-th retransmission with $r = \{1, 2, \cdots, k\}$, and $k = \{1, 2, \cdots, K\}$ is the current transmission index. The transmitter transmits a vectorized signal having N symbols, as $\mathbf{x}^{(k)} = [x_1^{(k)}, x_2^{(k)}, \cdots, x_N^{(k)}]^T \in \mathbb{C}^{N\times 1}$.

At the receiver side, the received signal vector $\mathbf{y}_k$ of the k-th transmitted frame is given by $\mathbf{y}^{(k)} = \mathbf{H}^{(k)}\mathbf{x}^{(k)} + \mathbf{v}^{(k)} \in \mathbb{C}^{N\times 1}$, where $\mathbf{v}_k$ is a zero mean complex AWGN vector with variance σ^2, corresponding to the received SNR. The channel is assumed to be static within a frame, and varies statistically independent frame-by-frame, because of the block fading assumption. The channel matrix $\mathbf{H}^{(k)}$ has a Toeplitz structure with

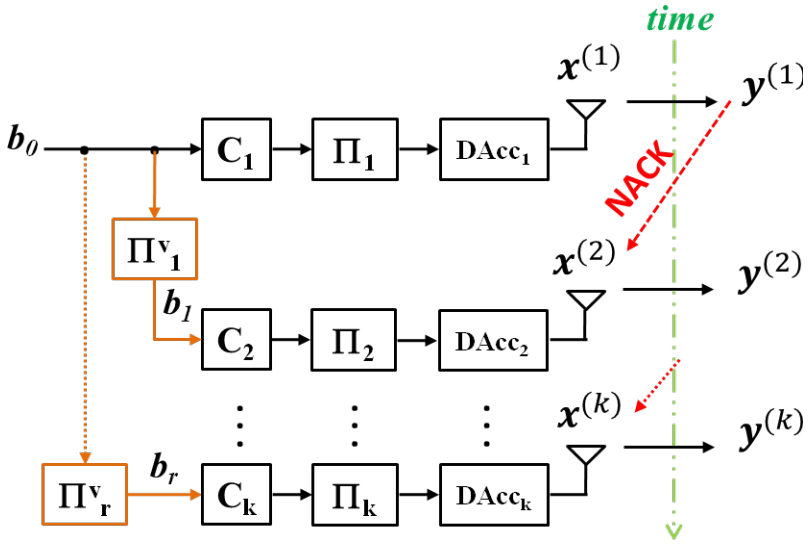

Figure 3.1. Transmitter of CAD Turbo HARQ Systems

the dimensionality $(N+L-1)\times N$, where L is the channel memory length. With the CP transmission, $\mathbf{H}^{(k)}$ becomes an $N\times N$ circulant matrix with the multipath channel response on its first column: $[h(0),h(1),\cdots,h(L-1),0,\cdots,0]^T$. Then, we can utilize the characteristic of the circularity to obtain a diagonal matrix of frequency domain channel matrix $\mathbf{\Psi}_k = \mathbf{F}^H\mathbf{H}_k\mathbf{F}$. This property is well utilized in the FD-SC/MMSE turbo equalization (EQ), as described in the previous chapter. The results of LLR are exchanged via *HI* between the equalizer+deaccumulator $(EQ+D_{DAcc})$ and the decoder (D). For the decoders D_{DAcc} and D, we use Bahl-Cocke-Jelinek-Raviv (BCJR) algorithm [24].

The *HI* takes place independently in different phases of transmission, as shown in Fig. 3.2. Therefore the channel matrix size stays the same at every *HI*. The *HI* is performed until no relevant improvement in MI is achieved, and then the obtained extrinsic LLR of the systematic information bits, $L^u_{e,D}$, is combined into L^u_s as

$$L^u_s = L^u_{e,D_1} + \sum_{i=2}^{k} \Pi^v_{i-1}(L^u_{e,D_i}), \tag{3.1}$$

L^u_s is fed back to soft-input soft-output (SISO) channel decoders as the *additional a priori* information, as depicted in Fig. 3.2, referred to as *VI*. The *VI* can be seen as iterative decoding process of PCC. Finally, by performing sufficient times of iterative

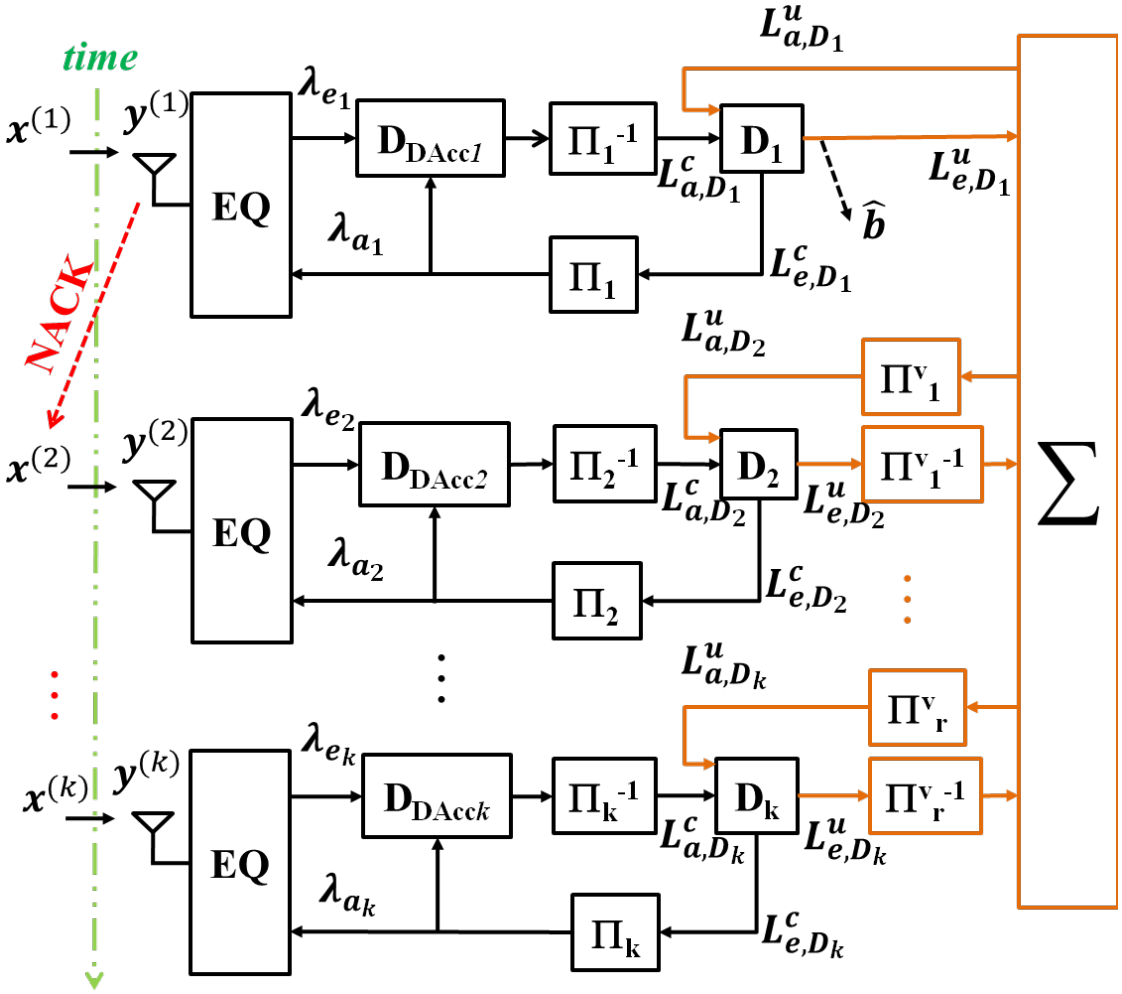

Figure 3.2. Receiver of CAD Turbo HARQ Systems

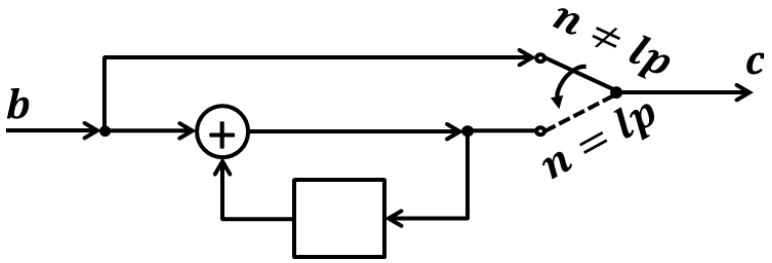

Figure 3.3. Doped-accumulator

HI-VI-HI-VI decoding, the final hard decision, $\hat{\mathbf{b}}$, is made on the *a posteriori* LLR of the information (systematic) bits.

3.1 Doped-accumulator

$DAcc$ is composed of a memory-1 systematic recursive convolutional code with octal generator of $([3,2]3)_8$ followed by heavy puncturing of the parity bits such that the coding rate is equal to one, as depicted in Fig.3.3. Every p-th systematic bits are replaced by the accumulated parity bits, where p without index indicates the doping rate in general, while p with the index k indicates the doping rate for the k-th transmission. As shown in Fig. 3.1, $DAcc$ is performed after the interleaver. At the receiver, D_{DAcc}, performed using the BCJR algorithm immediately after the FD-SC/MMSE equalization, as shown in Fig. 3.2. It should be noted that interleaver between D_{DAcc} and the equalizer is not needed because the extrinsic LLR is not iteratively exchanged between them.

3.2 EXIT Analysis

The structure of the CAD technique enables the use for different doping rates of the $DAcc$, transmission-by-transmission, to achieve better matching of the EXIT curves. The doping rate of the first transmission is determined by evaluating the EXIT curves of inner code (NSNRCC) and outer code $DAcc$ so that they are best matched among the all possible values of the doping rates, while keeping the convergence tunnel open until a point very close to the (1.0, 1.0) MI point. In such parameter settings, no retransmission is required if the received SNR is larger than the threshold at which the convergence tunnel opens.

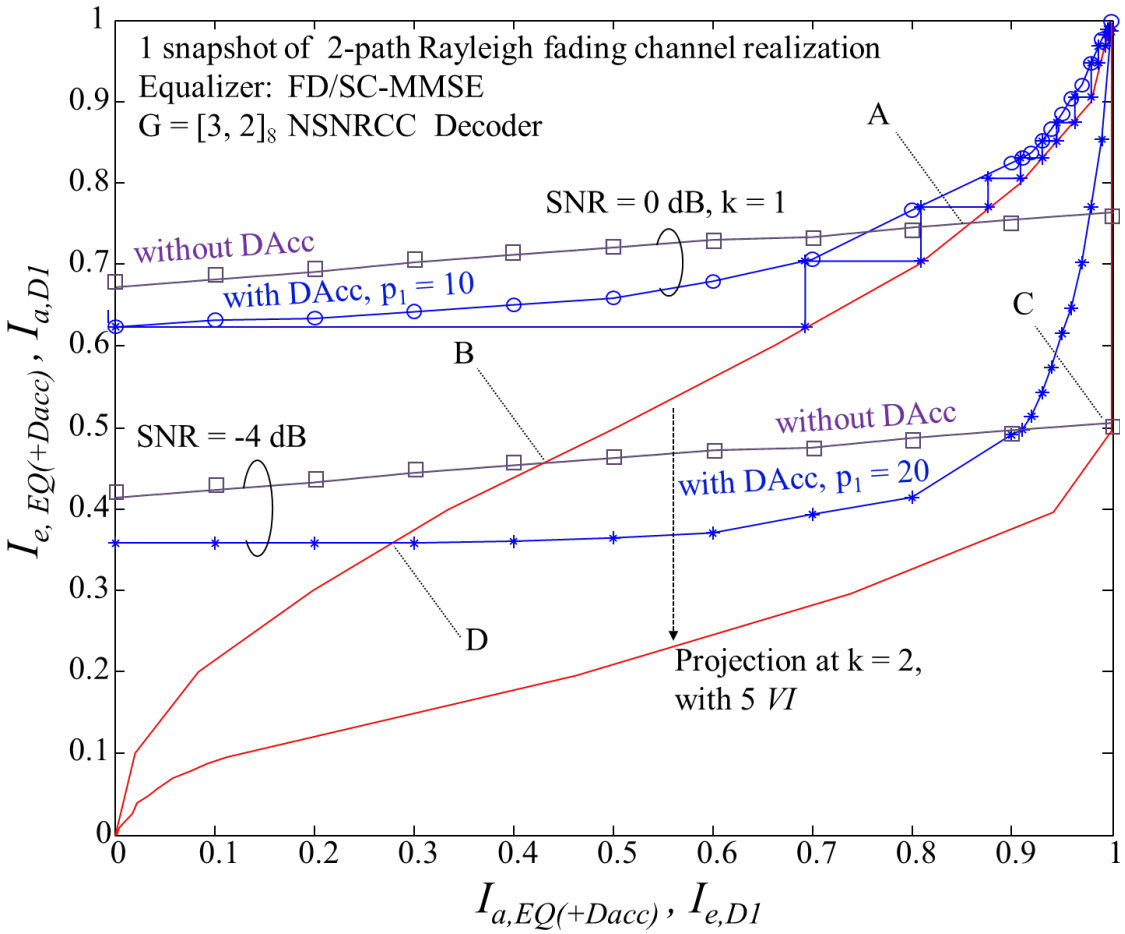

Figure 3.4. EXIT chart of Equalizer (+ D_{DAcc}) for single snapshot of channel realization and NSNRCC decoder at $k = \{1,2\}$

Fig. 3.4 shows the EXIT curves of EQ and $EQ + D_{DAcc}$, with a generator $[3,2]_8$ NSNRCC's decoder, for a single snapshot channel realization at the first transmission, and the same channel realization applies for retransmissions. The channel of the second transmission is generally different from the first, but in this figure we assume the same realization because the purpose of the EXIT analysis shown in this chapter is to demonstrate how the EXIT curve change by the *VI*. The figure also shows the trajectory with the maximum iteration of 350. We set the interleaver length to 20000 bits. For $k = 1$, we set the doping rate p_1 of $DAcc$ assisted CAD (ACC-CAD) to 10 and the average SNR to 0 dB. It shows that the EQ curve intersects the decoder curve at point "A", while $EQ + D_{DAcc}$ curve with $p_1 = 10$ makes the convergence tunnel open until a point very close to the (1.0,1.0) MI point.

At SNR = -4 dB, which is relatively low, the EQ curve intersects the decoder curve at point "B" whereas $EQ + D_{DAcc}$ curve with the doping rate $p_1 = 20$ intersects at the point "D" at which the attained MI is lower than at the point "B". Hence, with $p_1 = 20$, the performance of the system with $DAcc$ for the first transmission is worse than the system without $DAcc$. Furthermore, even though the MI at the intersection point can be raised by adjusting the doping rate, it is still difficult to reach a point close enough to the (1.0,1.0) MI point at the low SNR. CAD solve this problem with the help of *VI* that pushes down the decoder curve, resulting in better matching between $EQ + D_{DAcc}$ and decoder curves. Moreover, the gap between the two curves can further be reduced by adjusting the doping rate.

Chapter 4

Numerical Results

To evaluate the performances of the proposed HARQ technique, and to make performance comparison with other counterpart techniques, computer simulations has been conducted in AWGN and multipath Rayleigh fading channels. The results are presented in the this chapter. For the both scenarios, the following assumptions are used in common :

- the ARQ protocol is stop-and-wait,
- the rate of encoder is $R = 1/2$ for every phase of transmission
- CBD refers to the CBD-TDT technique [9], which is the an improved version of CBD-IEQ [7],
- CAD refers to the same structure as ACC-CAD but without $DAcc$
- in evaluation in multipath Rayleigh fading channel, fading complex envelops are complex Gaussian distributed i.i.d. random variable,
- the feedback channel is error free, and
- the packet error is perfectly detected.

For the fair comparison, we use the same memory size ($m = 2$) convolutional encoder, for the CBD and CAD, whereas the ACC-CAD use memory-1 convolutional encoder followed by $DAcc$ which is also memory-1 encoder. We perform simulations with maximum retransmission of 3 ($K = 4$). Results for $K = 3$ are not shown to simplify the figure. For fair comparison, we set the maximum iteration times at 350

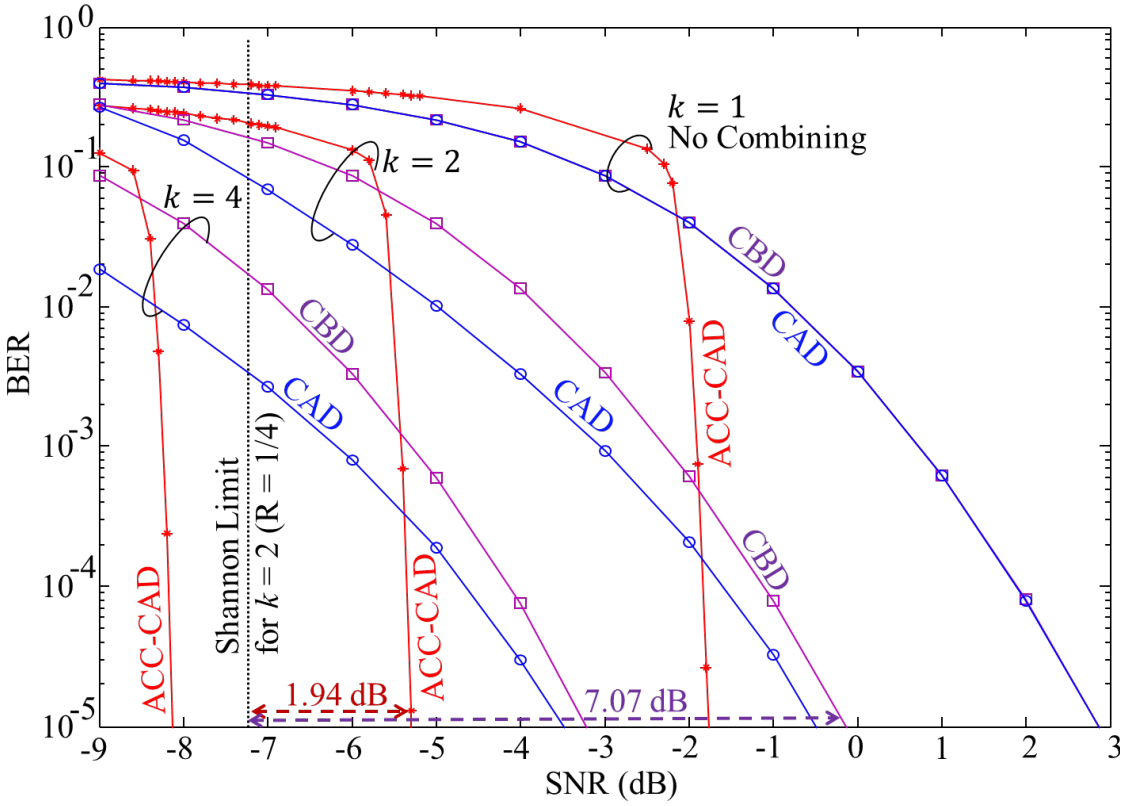

Figure 4.1. BER Performance in AWGN Channel

for every (re)transmission for all the tested systems.[1] Furthermore, the analysis of the computational complexity is provided in the last section of this chapter.

4.1 AWGN Channel

For AWGN channel case, 10000 information bits were generated for each frame and length 20000 bits of random interleaver were employed. The system models of CAD and CBD have the same structure of decoding for the first transmission and thereby the BER, FER, and throughput performances are same for $k = 1$ as shown in Fig. 4.1, Fig. 4.2, and Fig. 4.3, respectively. For $k > 1$, CAD outperforms CBD in BER, FER, and throughput performances. With ACC-CAD, employing $DAcc$ with doping rates $p_1 = 1$, $p_2 = 30$, $p_3 = 50$, and $p_4 = 65$, excellent improvement of CAD is achieved in BER, FER, and throughput performances. Furthermore, ACC-CAD results turbo cliff

[1]For *HI* and *VI*, the iteration are stopped when founding no relevant increase in the mutual information can be achieved after five consecutive iterations.

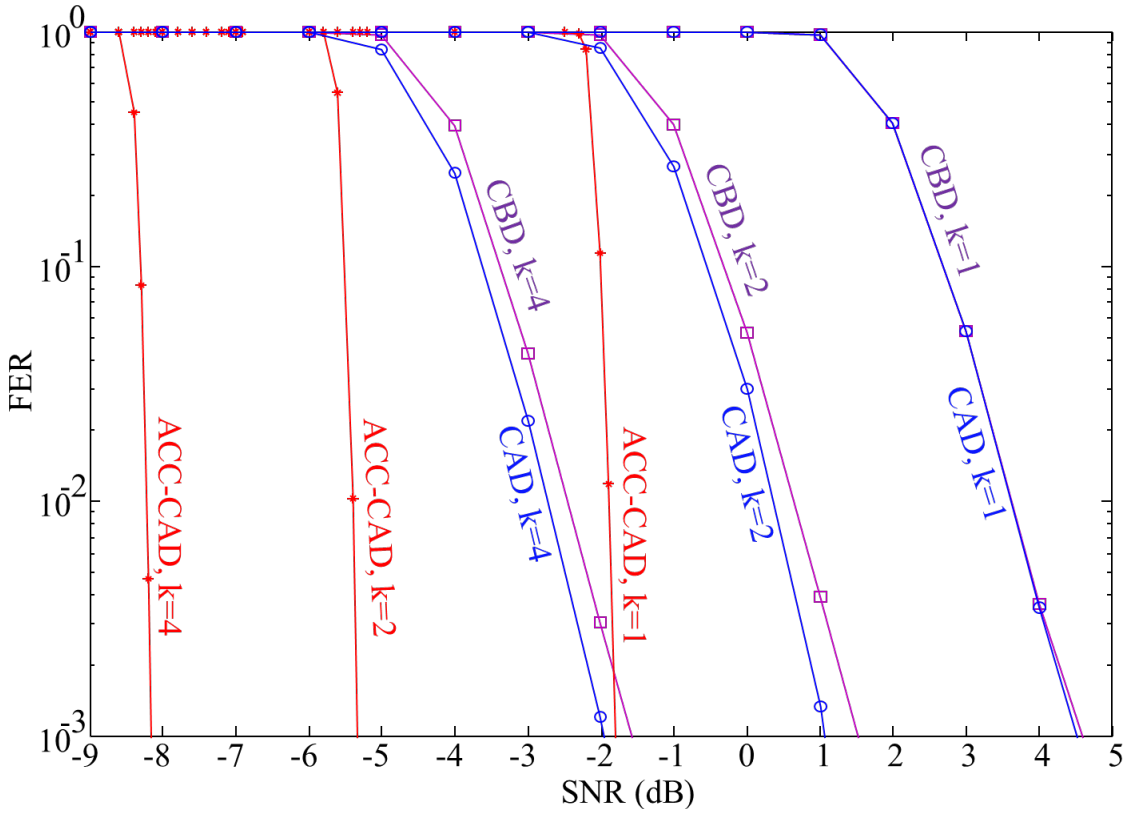

Figure 4.2. FER Performance in AWGN Channel

in performances because of the inner code, $DAcc$, makes the EXIT tunnel open and its EXIT curve varying only affected by SNR, whereas in multipath fading case by the channel realization varies transmission-by-transmission.

For $k = 2$, the BER performance of ACC-CAD shows clear turbo threshold at SNR 1.94 dB close to the Shannon limit corresponding to $R = 1/4$. At SNR < -5, which is relatively low, only ACC-CAD can achieve low FER and high throughput efficiency, as shown in Fig. 4.2 and Fig. 4.3, respectively. It is clear from Fig. 4.3 that with ACC-CAD, retransmission is *always* requested for SNR $\leq -2.4\ dB$, whereas with CBD the retransmission request is *always* performed for SNR $\leq 1\ dB$.

4.2 Multipath Fading Channel

For the performance evaluation in fading channel, we set 2-path i.i.d block fading channel with equal average path gains. Randomly generated binary sequence with a

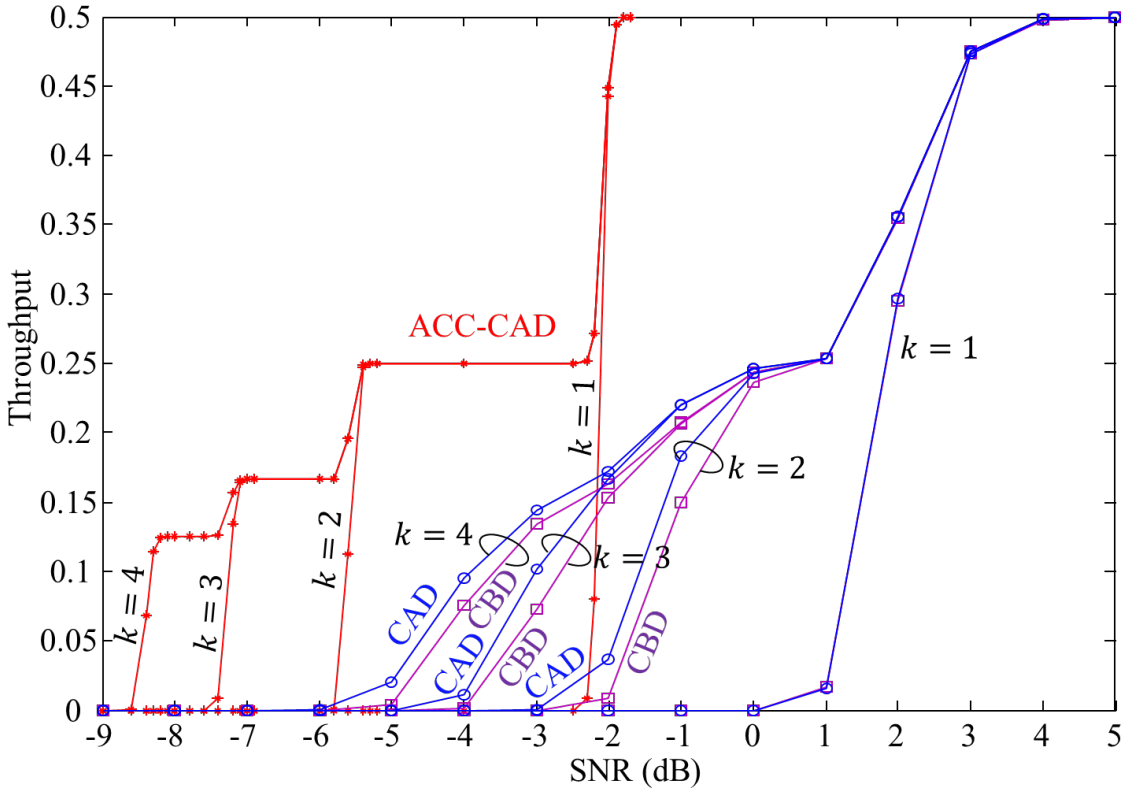

Figure 4.3. Throughput Performance in AWGN Channel

length of 512 information bits per frame were used as $\mathbf{b}_0$. Then, for ACC-CAD, $\mathbf{b}_0$ and $\mathbf{b}_r$ are independently coded by the same memory-1 rate $1/2$ NSNRCC encoder with generator polynomial $([3\ 2])_8$. For comparison, we also tested memory-2 rate $1/2$ NSNRCC encoder with generator polynomial $([7\ 5])_8$ for both CAD and CBD without $DAcc$. Here, the total memory number used for coding for all the evaluated systems is the same ($m = 2$).

With CAD, for $k = 2$, we perform first one *HI* in each branch then followed by five *VI*s; the *HI* and *VI* process are repeated 24 times, referred to as activation ordering pattern 24(H1V5). The activation ordering pattern for $k = 3$ and $k = 4$ are 16(H1V5) and 12(H1V5), respectively.

We evaluate the FER performances of the ACC-CAD with doping rates $p_1 = 10$, $p_2 = 20$, $p_3 = 50$, and $p_4 = 100$. These doping rates are different with those in AWGN's case because the channel varying influence the EXIT curve of $DAcc$ and thereby we obtained the doping rates by the brute-force approach for a channel realization. The outage probability curves of CBD and CAD, obtained from (2.25) and (2.25), respectively, are shown with dot line in Fig. 4.4. It is found that the decay of FER curves follow asymptotically those of the outage curves. For the first transmission (without combining), the both CAD and CBD systems schemes achieve the same outage probability. In this case, the system performance is determined by the path diversity and coding gains that can be achieved by the *HI* only.

It is found from Fig. 4.4 that the proposed CAD outperforms the systems without $DAcc$, as predicted from the EXIT analysis. With $k > 1$, the outage probability of CAD is lower than CBD; hence it is found that CAD clearly outperforms CBD. With ACC-CAD, the gap between FER and the outage probability, at FER $= 10^{-3}$ for $K = 2$, is 2.74 dB whereas with the CBD the gap is 4.56 dB. Similarly, for $K = 4$, the gap between the FER curve and the outage probability with the ACC-CAD is 3.18 dB whereas the CBD is 5.30 dB.

The excellent performance of the proposed systems is also demonstrated in terms of throughput efficiency at relatively low SNR in Fig. 4.5. With the ACC-CAD technique, as the throughput curves with every K value converge at SNR around 4 dB, we only need one retransmission, when SNR > 4 dB, to achieve the highest throughput. Fig. 4.5 also shows that ACC-CAD with only one retransmission outperforms the CBD with three retransmissions over the SNR value range of -2 dB $\leq$ SNR $\leq$ 8 dB in average.

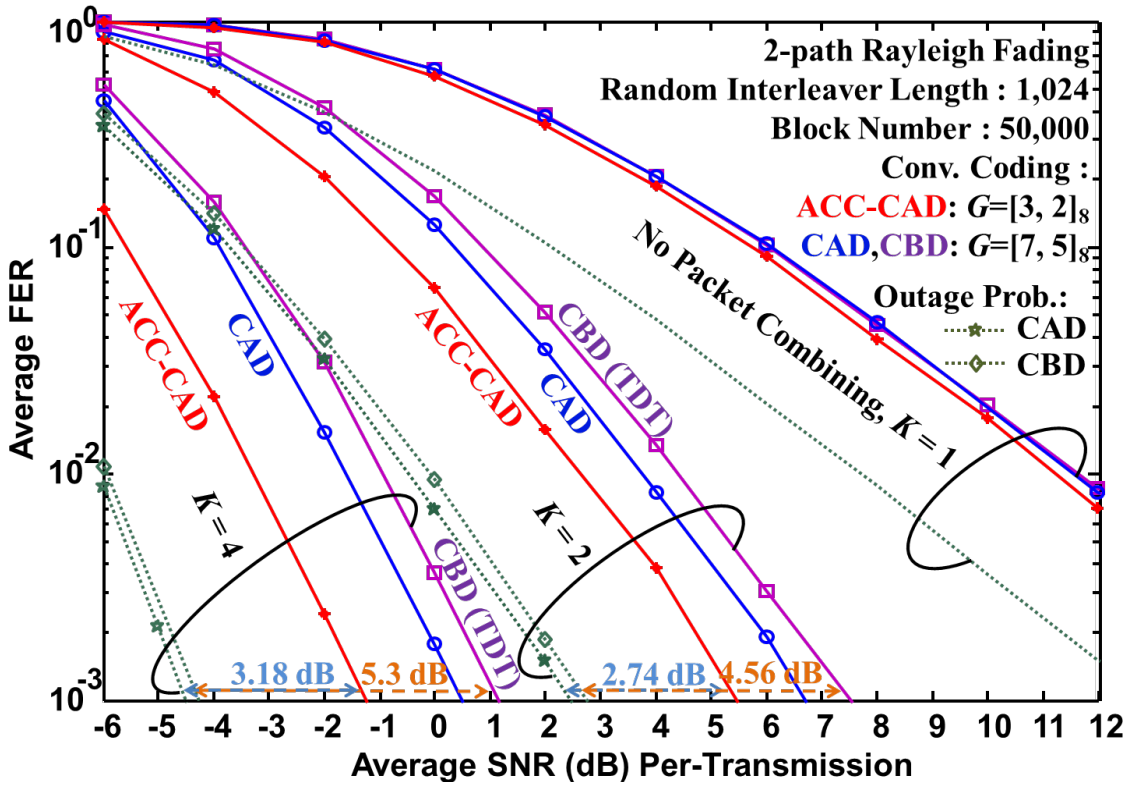

Figure 4.4. FER Performance in Multipath Fading Channel, $L = 2$

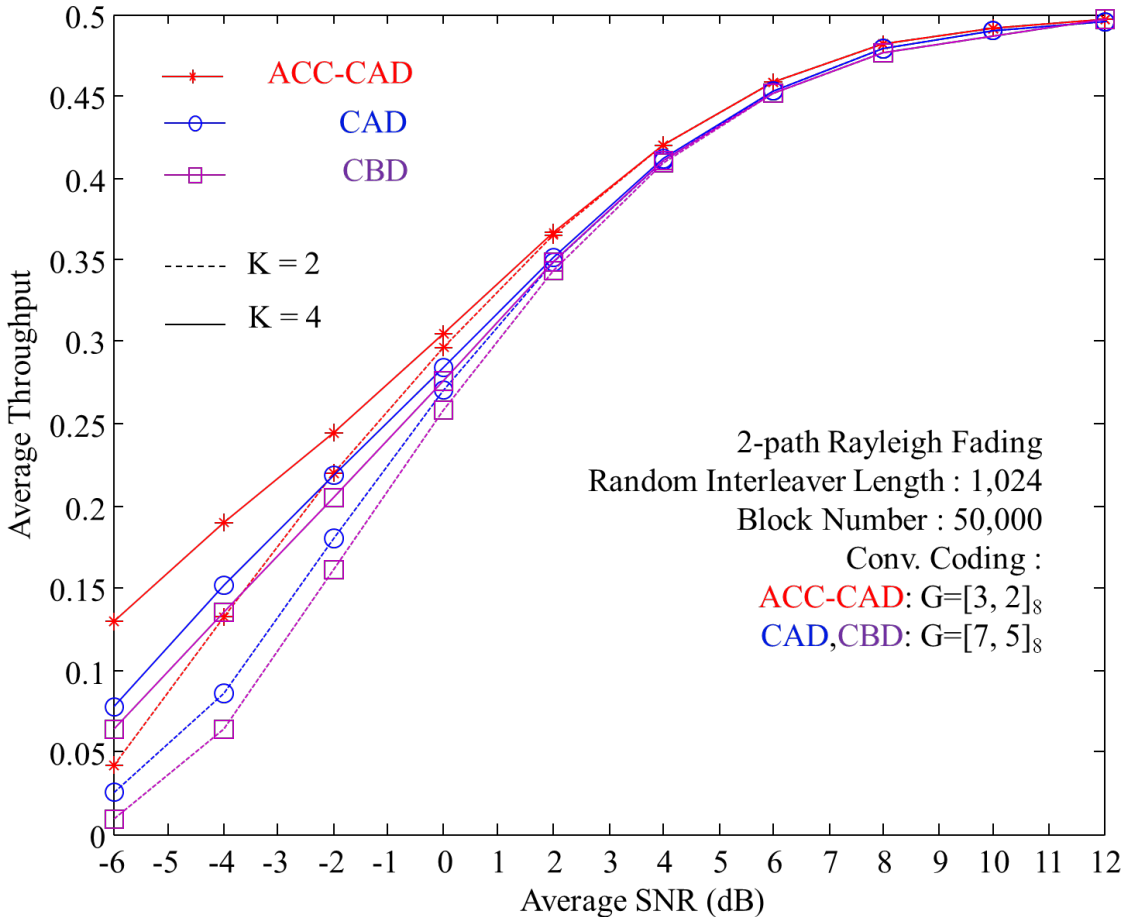

Figure 4.5. Throughput Performance in Multipath Fading Channel, $L = 2$

4.3 Complexity Comparison

Authors of Reference [25] define the Trellis complexity of a convolutional code as the number of symbols per coded bit, in the code trellis module. The Trellis complexity in symbols per bit is given by

$$C_x = \frac{n}{k} \times 2^{k+m}, \tag{4.1}$$

where $n, k,$ and m denote the number of coded bits, information bits, and memory, respectively. We use this measure which is directly related to the per-bit computational complexity of performing BCJR for MAP decoding of the used codes. Let $\kappa \geq 1$ denotes the κ-th transmission, the decoding complexity of the ACC-CAD, $C_{x,a}$, for $\kappa = 1$ is proportional to

$$C_{x,a}^{(1)} = i_h^{(1)} \times \frac{n}{k} \times 2^{k+m}, \tag{4.2}$$

where $i_h^{(1)}$ is the number of horizontal iterations used in the first transmission. Subsequently, the decoding complexity for the κ-th subsequent transmission, is proportional to

$$C_{x,a}^{(\kappa)} = i_h^{(\kappa)} \frac{n}{k} 2^{k+m} + i_{hv}^{(\kappa)} \left(\kappa\, i_v^{(\kappa)} \frac{n}{k} 2^{k+m} + \kappa\, i_h^{(\kappa)}\, 2 \frac{n}{k} 2^{k+m}\right) \tag{4.3}$$

which is equivalent to

$$C_{x,a}^{(\kappa)} = i_h^{(\kappa)} \frac{n}{k} 2^{k+m} + \kappa\, i_{hv}^{(\kappa)} \frac{n}{k} 2^{k+m} (i_v^{(\kappa)} + 2\, i_h^{(\kappa)}), \tag{4.4}$$

where $i_h^{(\kappa)}, i_v^{(\kappa)}, i_{hv}^{(\kappa)}$ denote the number of horizontal, vertical, and repetition of vertical + horizontal iterations, respectively. Let $\Upsilon = \frac{n}{k} 2^{k+m}$, the overall decoding complexity for the ACC-CAD is proportional to

$$C_{x,a} = i_h^{(1)} \Upsilon + (\kappa - 1)(i_h^{(\kappa)} \Upsilon + \kappa\, i_{hv}^{(\kappa)} \Upsilon (i_v^{(\kappa)} + 2\, i_h^{(\kappa)})) \tag{4.5}$$

On the other hand, the decoding complexity for the CBD, $C_{x,b}$, is basically the same for any transmissions, which is equal to (4.2), and hence the overall complexity

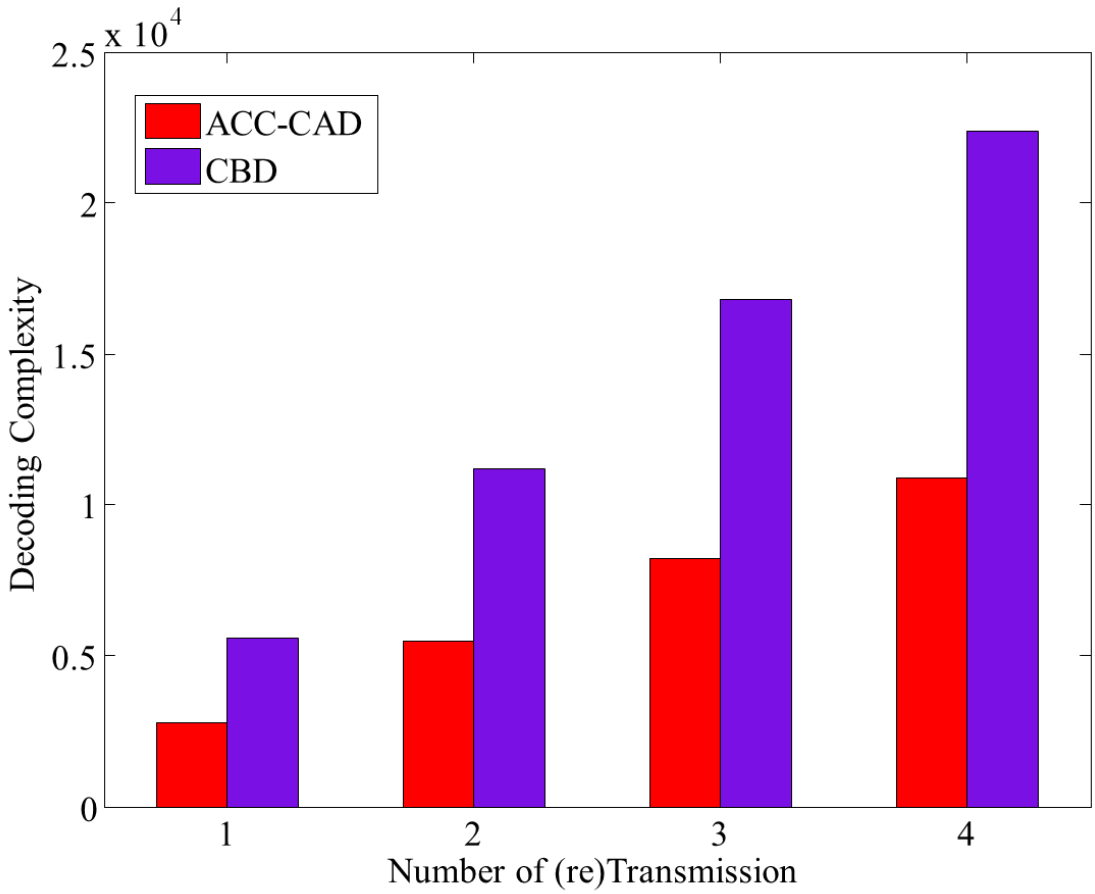

Figure 4.6. Complexity Comparison Between ACC-CAD and CBD

is proportional to

$$\begin{aligned} C_{x,b} &= i_h^{(\kappa)} \times \frac{n}{k} \times 2^{k+m} \\ &= i_h^{(\kappa)} \Upsilon. \end{aligned} \tag{4.6}$$

Fig. 4.6 shows[2] the decoding complexity comparison between ACC-CAD and CBD. It is found that ACC-CAD has less computational complexity than CBD.

[2]Complexity for the FD-SC/MMSE turbo equalizer is not included in the figure.

Chapter 5

Conclusions and Outlook

5.1 Conclusions

This thesis has proposed CAD HARQ technique using doped-accumulator ($DAcc$), assisted by *VI* decoding. It has been shown that the proposed system outperforms the HARQ systems without $DAcc$. With the help of EXIT chart analysis, a better matching between $EQ + D_{DAcc}$ and NRNSCC decoder's EXIT curves, concatenated with *VI* decoding, can be achieved with the proposed technique, which results in excellent FER and throughput performances. The superiority of CAD over CBD has also been verified via computer simulations in AWGN and multipath Rayleigh fading channels.

The main contributions that have been achieved in this research work are summarized as follows :

- $DAcc$ enables flexible adaptation to the channel conditions without requiring prohibitively large computational complexity by adjusting the doping rate while keeping close matching between the $EQ + D_{DAcc}$ and channel decoder EXIT curves.
- Additional coding gain, on the top of diversity gain, is achieved via *VI*.
- FER performance tendency and theoretical outage probability are consistent with each other, and the gap is roughly 2.76 dB.

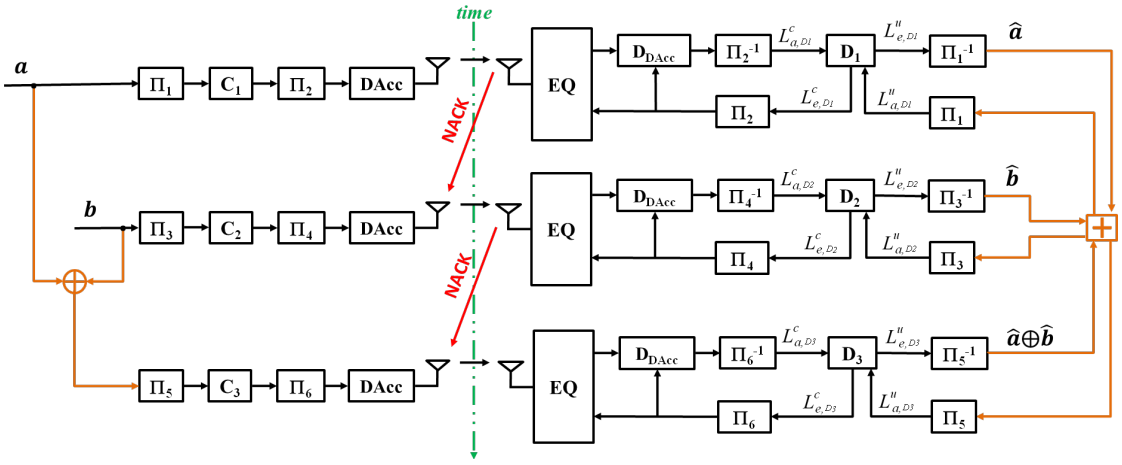

Figure 5.1. Network-Coding Assisted CAD Systems

5.2 Outlook

In the course of this work, numerous research problems have appeared or been left unsolved, among which the following are of particular interest :

- the problem of choosing the best $EQ + D_{DAcc}$ EXIT curve to be matched with the channel decoder curve can be optimized by formulating the EXIT curve in a mathematical way with which some numerical tools/algorithms can be used,
- it is possible to further extend and apply the proposed technique to the scenarios having network structures.
- network-coding assisted CAD transmission, where its system model is shown in Fig. 5.1, can be used for achieving higher throughput when the SNR value range of interest is relatively high, as demonstrated in Fig. 5.2.

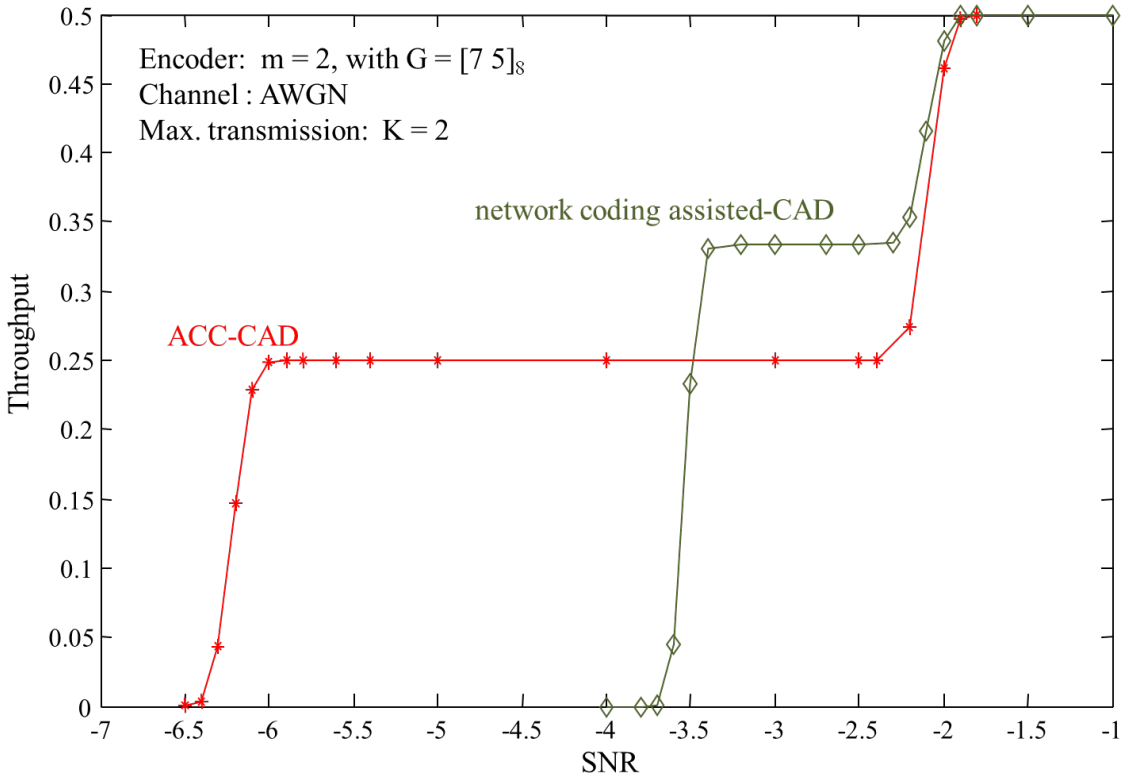

Figure 5.2. Throughput Performance of ACC-CAD and NC-CAD in AWGN Channel

Appendix A

CHATUE-OFDM Derivation

We redefine $\mathbf{y}$, $\mathbf{H}$, and $\mathbf{s}$ as received signal, channel response and transmitted signal, respectively. $\mathbf{s}'$ and $\mathbf{s}''$ are interferences component from the past and from the future of OFDM symbols, respectively. $\mathbf{H}'$ and $\mathbf{H}''$ are channel impulse response of the past and the future modes, respectively. We also define $\mathbf{F}$ as DFT and $\mathbf{F}^H$ IDFT.

The received signal of the current OFDM symbol, can be formulated as the following:

$$\mathbf{y} = \mathbf{H}'\mathbf{s}' + \mathbf{H}\mathbf{s} + \mathbf{H}''\mathbf{s}'' + \mathbf{v}, \tag{A.1}$$

where $\mathbf{v}$ denotes zero mean complex AWGN matrix with variance σ^2. $\mathbf{y}$ is multiplied by $\mathbf{J}$ matrix in order to get a circulant matrix so that (A.1) becomes

$$\mathbf{J}\mathbf{y} = \mathbf{J}\mathbf{H}'\mathbf{s}' + \mathbf{J}\mathbf{H}\mathbf{s} + \mathbf{J}\mathbf{H}''\mathbf{s}'' + \mathbf{J}\mathbf{v}. \tag{A.2}$$

After DFT, we will get :

$$\begin{aligned}
\mathbf{r} &= \mathbf{F}\mathbf{J}\mathbf{y} \\
\mathbf{r} &= \mathbf{F}\mathbf{J}\mathbf{H}'\mathbf{s}' + \mathbf{F}\mathbf{J}\mathbf{H}\mathbf{s} + \mathbf{F}\mathbf{J}\mathbf{H}''\mathbf{s}'' + \mathbf{F}\mathbf{J}\mathbf{v} \\
\mathbf{r} &= \mathbf{F}\mathbf{J}\mathbf{H}'\mathbf{F}^H\mathbf{x}' + \mathbf{F}\mathbf{J}\mathbf{H}\mathbf{F}^H\mathbf{x} + \mathbf{F}\mathbf{J}\mathbf{H}''\mathbf{F}^H\mathbf{x}'' + \mathbf{F}\mathbf{J}\mathbf{v},
\end{aligned} \tag{A.3}$$

where $\mathbf{x}$ is the data in the frequency domain and $\mathbf{r}$ is the input to the time domain SC/MMSE. Thus, equalization is performed in the frequency domain (FD).

We generate soft replica in FD-SC/MMSE as

$$\mathbf{p} = \mathbf{FJH}'\mathbf{F}^H\hat{\mathbf{x}}' + \mathbf{FJHF}^H\hat{\mathbf{x}} + \mathbf{FJH}''\mathbf{F}^H\hat{\mathbf{x}}''. \tag{A.4}$$

Hence, the input of the MMSE filter is given by

$$\tilde{\mathbf{r}} = \mathbf{r} - \mathbf{p} \tag{A.5}$$

$$\begin{aligned}\tilde{\mathbf{r}} =& \mathbf{FJH}'\mathbf{F}^H(\mathbf{x}' - \hat{\mathbf{x}}') + \mathbf{FJHF}^H(\mathbf{x} - \hat{\mathbf{x}}) \\ &+ \mathbf{FJH}''\mathbf{F}^H(\mathbf{x}'' - \hat{\mathbf{x}}'') + \mathbf{FJv}.\end{aligned} \tag{A.6}$$

If *a priori* information is perfect, only noise component remains. Thus, in the second step of SC/MMSE, we introduce restoral term $\phi(n)\hat{x}(n)$, where $\phi(n)$ is the n-th column vector of

$$\mathbf{\Phi} = \mathbf{FJHF}^H \tag{A.7}$$

The size of $\phi(n)$ is $(\mathcal{N} \times 1)$, where $\mathcal{N}$ denotes OFDM symbol length. Let $\hat{x}(n)$ be the signal sample of the n-th subcarrier of current OFDM symbol vector $\hat{\mathbf{x}}$. Thus, we define the soft cancellation output $\hat{\mathbf{r}}(n)$ having restoral term for the n-th subcarrier, as

$$\hat{\mathbf{r}}(n) = \tilde{\mathbf{r}} + \phi(n)\hat{x}(n). \tag{A.8}$$

Then, $\hat{\mathbf{r}}(n)$ is multiplied by weighting factor $\mathbf{w}$ so that we have the filter output as $z(n) = \mathbf{w}^H(n)\hat{\mathbf{r}}(n)$, for which the criterion is given by

$$\mathbf{w} = arg\, min_{\mathbf{w}^H(n)} E\Big\{ \Big\| x(n) - \mathbf{w}^H(n)\hat{\mathbf{r}}(n) \Big\|^2 \Big\}. \tag{A.9}$$

By utilizing the Wiener-Hopf method, the solution to (A.9) is given by

$$E\left[\frac{\partial}{\partial \mathbf{w}^H(n)} \Big\| x(n) - \mathbf{w}^H(n)\hat{\mathbf{r}}(n) \Big\|^2 \right] = 0. \tag{A.10}$$

We then obtain

$$E\left[\frac{\partial}{\partial \mathbf{w}^H(n)} (x(n) - \mathbf{w}^H(n)\hat{\mathbf{r}}(n))(x(n) - \mathbf{w}^H(n)\hat{\mathbf{r}}(n))^H \right] = 0,$$

which is equivalent to

$$E\left[\frac{\partial}{\partial \mathbf{w}^H(n)}(x(n)-\mathbf{w}^H(n)\hat{\mathbf{r}}(n))(x^*(n)-\hat{\mathbf{r}}^H(n)\mathbf{w}(n))\right]=0,$$

yielding the solution :

$$E\left[\hat{\mathbf{r}}(n)\hat{\mathbf{r}}^H(n)\right]\mathbf{w}(n)-E\left[\hat{\mathbf{r}}(n)x^*(n)\right]=0. \tag{A.11}$$

The first expectation of (A.11) is calculated as follows

$$\begin{aligned}
E\left[\hat{\mathbf{r}}(n)\hat{\mathbf{r}}^H(n)\right] =& E\left[(\tilde{\mathbf{r}}+\phi(n)\hat{x}(n))(\tilde{\mathbf{r}}+\phi(n)\hat{x}(n))^H\right]\\
=& E\left[(\tilde{\mathbf{r}}+\phi(n)\hat{x}(n))(\tilde{\mathbf{r}}^H+\hat{x}^*(n)\phi^H(n))\right]\\
=& E\Big[(\tilde{\mathbf{r}}\tilde{\mathbf{r}}^H+\tilde{\mathbf{r}}\hat{x}^*(n)\phi^H(n)+\phi(n)\hat{x}(n)\tilde{\mathbf{r}}^H\\
&+\phi(n)\hat{x}(n)\hat{x}^*(n)\phi^H(n))\Big]\\
=& E\left[\tilde{\mathbf{r}}\tilde{\mathbf{r}}^H+\phi(n)|\hat{x}(n)|^2\phi^H(n)\right]\\
=& E\left[\tilde{\mathbf{r}}\tilde{\mathbf{r}}^H\right]+\phi(n)|\hat{x}(n)|^2\phi^H(n).
\end{aligned} \tag{A.12}$$

We assume that OFDM symbols are uncorrelated, and thereby we can calculate $E[\tilde{\mathbf{r}}\tilde{\mathbf{r}}^H]$ as

$$\begin{aligned}
E\left[\tilde{\mathbf{r}}\tilde{\mathbf{r}}^H\right] =& E\Big[(\mathbf{FJH}'\mathbf{F}^H(\mathbf{x}'-\hat{\mathbf{x}}')+\mathbf{FJHF}^H(\mathbf{x}-\hat{\mathbf{x}})+\mathbf{FJH}''\mathbf{F}^H(\mathbf{x}''-\hat{\mathbf{x}}'')\\
&+\mathbf{FJv})\\
&(\mathbf{FJH}'\mathbf{F}^H(\mathbf{x}'-\hat{\mathbf{x}}')+\mathbf{FJHF}^H(\mathbf{x}-\hat{\mathbf{x}})+\mathbf{FJH}''\mathbf{F}^H(\mathbf{x}''-\hat{\mathbf{x}}'')\\
&+\mathbf{FJv})^H\Big]\\
=& E\Big[(\mathbf{FJH}'\mathbf{F}^H(\mathbf{x}'-\hat{\mathbf{x}}')+\mathbf{FJHF}^H(\mathbf{x}-\hat{\mathbf{x}})+\mathbf{FJH}''\mathbf{F}^H(\mathbf{x}''-\hat{\mathbf{x}}'')\\
&+\mathbf{FJv})\\
&((\mathbf{FJH}'\mathbf{F}^H(\mathbf{x}'-\hat{\mathbf{x}}'))^H+(\mathbf{FJHF}^H(\mathbf{x}-\hat{\mathbf{x}}))^H
\end{aligned}$$

$$
\begin{aligned}
&+ (\mathbf{FJH}''\mathbf{F}^H(\mathbf{x}'' - \hat{\mathbf{x}}''))^H + (\mathbf{FJv})^H)\Big] \\
=&E\Big[\mathbf{FJH}'\mathbf{F}^H(\mathbf{x}' - \hat{\mathbf{x}}')\,(\mathbf{x}' - \hat{\mathbf{x}}')^H\,(\mathbf{FJH}'\mathbf{F}^H)^H\Big] \\
&+ E\Big[\mathbf{FJHF}^H(\mathbf{x} - \hat{\mathbf{x}})\,(\mathbf{x} - \hat{\mathbf{x}})^H\,(\mathbf{FJHF}^H)^H\Big] \\
&+ E\Big[\mathbf{FJH}''\mathbf{F}^H(\mathbf{x}'' - \hat{\mathbf{x}}'')\,(\mathbf{x}'' - \hat{\mathbf{x}}'')^H\,(\mathbf{FJH}''\mathbf{F}^H)^H\Big] \\
&+ E\Big[(\mathbf{FJv})(\mathbf{FJv})^H\Big] \\
=&\mathbf{FJH}'\mathbf{F}^H\,E\Big[(\mathbf{x}' - \hat{\mathbf{x}}')\,(\mathbf{x}' - \hat{\mathbf{x}}')^H\Big]\,(\mathbf{FJH}'\mathbf{F}^H)^H \\
&+ \mathbf{FJHF}^H\,E\Big[(\mathbf{x} - \hat{\mathbf{x}})\,(\mathbf{x} - \hat{\mathbf{x}})^H\Big]\,(\mathbf{FJHF}^H)^H \\
&+ \mathbf{FJH}''\mathbf{F}^H\,E\Big[(\mathbf{x}'' - \hat{\mathbf{x}}'')\,(\mathbf{x}'' - \hat{\mathbf{x}}'')^H\Big]\,(\mathbf{FJH}''\mathbf{F}^H)^H \\
&+ \mathbf{F}\sigma^2\mathbf{JJ}^H\mathbf{F}^H. \qquad \text{(A.13)}
\end{aligned}
$$

Therefore, (A.12) becomes

$$E\Big[\hat{\mathbf{r}}(n)\hat{\mathbf{r}}^H(n)\Big] = \mathbf{\Sigma} + \phi(n)|\hat{x}(n)|^2\phi^H(n), \qquad \text{(A.14)}$$

where

$$
\begin{aligned}
\mathbf{\Sigma} =&\mathbf{FJH}'\mathbf{F}\lambda'(\mathbf{FJH}'\mathbf{F})^H + \mathbf{FJHF}\lambda(\mathbf{FJHF})^H + \mathbf{FJH}''\mathbf{F}\lambda''(\mathbf{FJH}''\mathbf{F})^H \\
&+ \mathbf{F}\sigma^2\mathbf{JJ}^H\mathbf{F}^H, \qquad \text{(A.15)}
\end{aligned}
$$

with

$$\lambda' = E\Big[(\mathbf{x}' - \hat{\mathbf{x}}')\,(\mathbf{x}' - \hat{\mathbf{x}}')^H\Big]. \qquad \text{(A.16)}$$

By using BPSK format of modulation, the average power of the transmitted signal is equal to 1, and thereby (A.16) become

$$\lambda' = E\Big[(\mathbf{1} - \hat{\mathbf{x}}')\,(\mathbf{1} - \hat{\mathbf{x}}')^H\Big]. \qquad \text{(A.17)}$$

The last expectation of (A.11) is calculated as

$$\begin{aligned}
E\left[\hat{\mathbf{r}}(n)x^*(n)\right] =& E\left[(\tilde{\mathbf{r}}+\phi(n)\hat{x}(n))x^*(n)\right] \\
=& E\left[\tilde{\mathbf{r}}x^*(n)+\phi(n)\hat{x}(n)x^*(n)\right] \\
=& E\Big[(\mathbf{FJH'F}^H(\mathbf{x'}-\hat{\mathbf{x}}')+\mathbf{FJHF}^H(\mathbf{x}-\hat{\mathbf{x}}) \\
& +\mathbf{FJH''F}^H(\mathbf{x''}-\hat{\mathbf{x}}'')+\mathbf{FJv})x^*(n)+\phi(n)\hat{x}(n)x^*(n)\Big] \\
=& E\left[\mathbf{FJHF}(\mathbf{x}-\hat{\mathbf{x}})x^*(n)+\mathbf{FJv}x^*(n)+\phi(n)\hat{x}(n)x^*(n)\right] \\
=& E\left[\phi(n)\hat{x}(n)x^*(n)\right] \\
=& \phi(n). \qquad \text{(A.18)}
\end{aligned}$$

The optimum filter tap coefficients can be found by using (A.11), (A.14), and (A.18), as

$$\mathbf{w}(n) = (\mathbf{\Sigma}+\phi(n)|\hat{x}(n)|^2\phi^H(n))^{-1}\phi(n), \qquad \text{(A.19)}$$

which is equivalent to

$$\begin{aligned}
\mathbf{w}^H(n) &= ((\mathbf{\Sigma}+\phi(n)|\hat{x}(n)|^2\phi^H(n))^{-1}\phi(n))^H \\
&= \phi^H(n)((\mathbf{\Sigma}+\phi(n)|\hat{x}(n)|^2\phi^H(n))^{-1})^H \\
&= \phi^H(n)(\mathbf{\Sigma}+\phi(n)|\hat{x}(n)|^2\phi^H(n))^{-1}. \qquad \text{(A.20)}
\end{aligned}$$

By using matrix inversion lemma :
$[A+BCD]^{-1} = A^{-1} - A^{-1}B[C^{-1}+DA^{-1}B]^{-1}DA^{-1}$,
we can decompose (A.20) as the following

$$\begin{aligned}
\mathbf{w}^H(n) &= \phi^H(n)(\mathbf{\Sigma}+\phi(n)|\hat{x}(n)|^2\phi^H(n))^{-1} \\
&= \phi^H(n)(\mathbf{\Sigma}^{-1}-\mathbf{\Sigma}^{-1}\phi(n)\left[(|\hat{x}(n)|^2)^{-1}+\phi^H(n)\mathbf{\Sigma}^{-1}\phi(n)\right]^{-1}\phi^H(n)\mathbf{\Sigma}^{-1}) \\
&= \phi^H(n)\mathbf{\Sigma}^{-1}-\phi^H(n)\mathbf{\Sigma}^{-1}\phi(n)\left[(|\hat{x}(n)|^2)^{-1}+\phi^H(n)\mathbf{\Sigma}^{-1}\phi(n)\right]^{-1}\phi^H(n)\mathbf{\Sigma}^{-1} \\
&= \phi^H(n)\mathbf{\Sigma}^{-1}-\gamma(n)\left[|\hat{x}(n)|^{-2}+\gamma(n)\right]^{-1}\phi^H(n)\mathbf{\Sigma}^{-1},
\end{aligned}$$

which, with the help of the definition $\gamma(n) = \phi^H(n)\mathbf{\Sigma}^{-1}\phi(n)$, can further be reduced to

$$\begin{aligned}
\mathbf{w}^H(n) &= \phi^H(n)\mathbf{\Sigma}^{-1} - \frac{\gamma(n)}{|\hat{x}(n)|^{-2} + \gamma(n)}\phi^H(n)\mathbf{\Sigma}^{-1} \\
&= \phi^H(n)\mathbf{\Sigma}^{-1} - \frac{\gamma(n)|\hat{x}(n)|^2}{1 + \gamma(n)|\hat{x}(n)|^2}\phi^H(n)\mathbf{\Sigma}^{-1} \\
&= \left(1 - \frac{\gamma(n)|\hat{x}(n)|^2}{1 + \gamma(n)|\hat{x}(n)|^2}\right)\phi^H(n)\mathbf{\Sigma}^{-1} \\
&= \left(1 + \gamma(n)|\hat{x}(n)|^2\right)^{-1}\phi^H(n)\mathbf{\Sigma}^{-1} \qquad \text{(A.21)}
\end{aligned}$$

Therefore, the output of SC/MMSE is given by

$$\begin{aligned}
z(n) &= \mathbf{w}^H(n)\hat{\mathbf{r}}(n) \\
&= \left(1 + \gamma(n)|\hat{x}(n)|^2\right)^{-1}\phi^H(n)\mathbf{\Sigma}^{-1}(\tilde{\mathbf{r}} + \phi(n)\hat{x}(n)) \\
&= \left(1 + \gamma(n)|\hat{x}(n)|^2\right)^{-1}(\phi^H(n)\mathbf{\Sigma}^{-1}\tilde{\mathbf{r}} + \phi^H(n)\mathbf{\Sigma}^{-1}\phi(n)\hat{x}(n)) \\
&= \left(1 + \gamma(n)|\hat{x}(n)|^2\right)^{-1}(\phi^H(n)\mathbf{\Sigma}^{-1}\tilde{\mathbf{r}} + \gamma(n)\hat{x}(n)), \qquad \text{(A.22)}
\end{aligned}$$

with block-wise expression

$$\mathbf{z} = (\mathbf{I}_{K,K} + \mathbf{\Gamma}\mathbf{X})^{-1}(\mathbf{\Phi}\mathbf{\Sigma}^{-1}\tilde{\mathbf{r}} + \mathbf{\Gamma}\hat{x}), \qquad \text{(A.23)}$$

where

$$\begin{aligned}
\mathbf{\Gamma} &= \bar{diag}\left[\mathbf{\Phi}^H\mathbf{\Sigma}^{-1}\mathbf{\Phi}\right], \\
\mathbf{X} &= \bar{diag}\left[\hat{x}\right],
\end{aligned}$$

$\bar{diag}$ denotes a diagonal matrix constructed by its argument vector, having its diagonal elements being the elements of the argument vector, and the rest being zeros.

It is assumed that the output $z(n)$ can be expressed as

$$z(n) = \mu(n)x(n) + v(n),$$

where

$$\begin{aligned}\mu(n) &= E[z(n)x^*(n)] \\ &= \frac{\gamma(n)}{1+\gamma(n)|\hat{x}(n)|^2}E[|\hat{x}(n)|^2],\end{aligned}$$

and the variance of $v(n)$ is given by

$$\begin{aligned}\sigma^2(n) &= E[z(n)z^*(n)] - \mu^2(n) \\ &= \mu(n)(1-\mu(n)),\end{aligned}$$

hence, the output of the equalizer expressed in extrinsic LLR is given by

$$\begin{aligned}\lambda[x(n)] &= ln\left(\frac{Prob.[z(n)|x(n)=+1]}{Prob.[z(n)|x(n)=-1]}\right) \\ &= ln\left(\frac{exp\left[-\frac{|\Re[z(n)]-\mu(n)|^2}{2\sigma^2(n)/2}\right]}{exp\left[-\frac{|\Re[z(n)]+\mu(n)|^2}{2\sigma^2(n)/2}\right]}\right) \\ &= \frac{4\mu(n)\Re[z(n)]}{\mu(n)(1-\mu(n))} \\ &= \frac{4\Re[z(n)]}{1-\mu(n)}\end{aligned}$$

Appendix B

CHATUE-MU-SIMO-OFDM Derivation

In Appendix B, only parts which makes fundamental of difference between CHATUE-OFDM and CHATUE-MU-SIMO-OFDM signalling schemes are shown below.

Instead of column-wise calculation of restoral term in the soft cancellation process as introduced for the CHATUE-OFDM systems, we use block restoral term $\mathbf{\Phi}\hat{\mathbf{x}}_t$ where $\mathbf{\Phi}$ is a block diagonal matrix given by

$$\mathbf{\Phi} = \mathbf{FJH}_t\mathbf{F}^H \in \mathbb{C}^{\mathcal{N}K_R \times \mathcal{N}K_R} \tag{B.1}$$

Accordingly, the input of MMSE filter is given by

$$\begin{aligned}\bar{\mathbf{y}}_t = &\ \tilde{\mathbf{y}}_t + \mathbf{\Phi}\hat{\mathbf{x}}_t \\ = &\ \mathbf{FJH}'_{t-1}\mathbf{F}^H(\mathbf{x}'_{t-1} - \hat{\mathbf{x}}'_{t-1}) + \mathbf{FJH}_t\mathbf{F}^H(\mathbf{x}_t - \hat{\mathbf{x}}_t) \\ &+ \mathbf{FJH}''_{t+1}\mathbf{F}^H(\mathbf{x}''_{t+1} - \hat{\mathbf{x}}''_{t+1}) + \mathbf{FJn} + \mathbf{FJH}_t\mathbf{F}^H\hat{\mathbf{x}}_t \in \mathbb{C}^{\mathcal{N}K_R \times 1}\end{aligned} \tag{B.2}$$

With the aid of matrix inversion lemma further weights for MMSE filtering is obtained as leads to the following expression

$$\mathbf{W}^H = \left(\mathbf{1}_{\mathcal{N}K_T \times \mathcal{N}K_R} + \Gamma\hat{\mathbf{X}}_t\right)^{-1}\mathbf{\Phi}^H\mathbf{\Sigma}^{-1} \in \mathbb{C}^{\mathcal{N}K_R \times \mathcal{N}K_R} \tag{B.3}$$

where $\hat{\mathbf{X}}_t$ is a covariance matrix of $\hat{\mathbf{x}}_t$, $\Gamma = \mathbf{\Phi}^H \mathbf{\Sigma}^{-1} \mathbf{\Phi}$, and $\mathbf{\Sigma}$ is given by

$$\begin{aligned}\mathbf{\Sigma} = \; & \mathbf{FJH}'_{t-1}\mathbf{F}^H \mathbf{\Lambda}'_{t-1} (\mathbf{FJH}'_{t-1}\mathbf{F}^H)^H + \mathbf{FJH}_t \mathbf{F}^H \mathbf{\Lambda}_t (\mathbf{FJH}_t \mathbf{F}^H)^H \\ & + \mathbf{FJH}''_{t+1}\mathbf{F}^H \mathbf{\Lambda}''_{t+1} (\mathbf{FJH}''_{t+1}\mathbf{F}^H)^H + \mathbf{F}\sigma^2 \mathbf{J}\mathbf{J}^H \mathbf{F}^H \in \mathbb{C}^{\mathcal{N}K_R \times \mathcal{N}K_R}, \end{aligned} \tag{B.4}$$

with covariance matrices of the ISI components remaining in the current frame after the soft cancellation, as

$$\begin{aligned} \mathbf{\Lambda}'_{t-1} &= E\left[(\mathbf{x}'_{t-1} - \hat{\mathbf{x}}'_{t-1}) (\mathbf{x}'_{t-1} - \hat{\mathbf{x}}'_{t-1})^H \right] \in \mathbb{C}^{\mathcal{N}K_T \times \mathcal{N}K_T}, \\ \mathbf{\Lambda}_t &= E\left[(\mathbf{x}_t - \hat{\mathbf{x}}_t) (\mathbf{x}_t - \hat{\mathbf{x}}_t)^H \right] \in \mathbb{C}^{\mathcal{N}K_T \times \mathcal{N}K_T}, \\ \mathbf{\Lambda}''_{t+1} &= E\left[(\mathbf{x}''_{t+1} - \hat{\mathbf{x}}''_{t+1}) (\mathbf{x}''_{t+1} - \hat{\mathbf{x}}''_{t+1})^H \right] \in \mathbb{C}^{\mathcal{N}K_T \times \mathcal{N}K_T}, \end{aligned} \tag{B.5}$$

and the noise variance denoted by σ^2. Finally, the equalizer output can be obtained by using (B.2) and (B.3) as

$$\begin{aligned} \mathbf{z} = \mathbf{W}^H \bar{\mathbf{y}} &= \left(\mathbf{1}_{\mathcal{N}K_T \times \mathcal{N}K_R} + \Gamma \hat{\mathbf{X}} \right)^{-1} \mathbf{\Phi}^H \mathbf{\Sigma}^{-1} (\tilde{\mathbf{y}} + \mathbf{\Phi}\hat{\mathbf{x}}) \\ &= \left(\mathbf{1}_{\mathcal{N}K_T \times \mathcal{N}K_R} + \Gamma \hat{\mathbf{X}} \right)^{-1} (\mathbf{\Phi}^H \mathbf{\Sigma}^{-1} \tilde{\mathbf{y}} + \Gamma \hat{\mathbf{x}}) \in \mathbb{C}^{\mathcal{N}K_R \times 1} \end{aligned} \tag{B.6}$$

Appendix C

CHATUE-OFDM Performances

In Appendix C, only figures indicating performances of single-user and multiuser CHATUE-OFDM are provided with short descriptions for the performance tendencies. This is because the main focus of this thesis is not OFDM but HARQ, where single carrier FD-SC/MMSE is a core part, as described in the main body. Nevertheless, single carrier FD-SC/MMSE and CHATUE-OFDM are closely connected, as described in Subsection 2.6.1 and hence we derive the CHATUE-OFDM algorithm based on the single carrier FD-SC/MMSE algorithm. Furthermore, the CHATUE-OFDM research has been financially supported by the project sponsors, SANYO Electric Co., Ltd and Kinki Mobile Radio Center Inc, and therefore we believe it is reasonable to provide the main results of the project in this thesis.

C.1 Single-user's Case

Fig. 2.14 shows the considered system model of the CHATUE-OFDM for single user's case. The system parameters are summarized in Table C.1. We asses performances of OFDM with GI and without GI. To make a fair comparison, a puncturing is used by OFDM transmitter to keep the same symbol duration of OFDM with GI and without GI.

Fig. C.1 shows that with the same spectral efficiency, OFDM system without GI can improve the BER performance by about 14 dB for $R = 4/7$ and 20 dB for $R = 2/3$ with BER 10^{-5}.

Table C.1. Simulation Parameters of CHATUE for Single User OFDM

Transmitter	Modulation	BPSK
	Subcarriers (FFT size)	512, no training sub-carriers
	Encoder	Convolutional Codes with GP = [5,7]
		R = 1/2, 2/3, 4/7
	Interleaver	Random
	doping rate	1/4
Channel	Multipath Fading	64 paths, Jakes Model
Receiver	Equalizer	FD/SC-MMSE
	Iterations	10
	Channel Estimation	Perfect
	Synchronization	Perfect
	Decoder	log-MAP BCJR

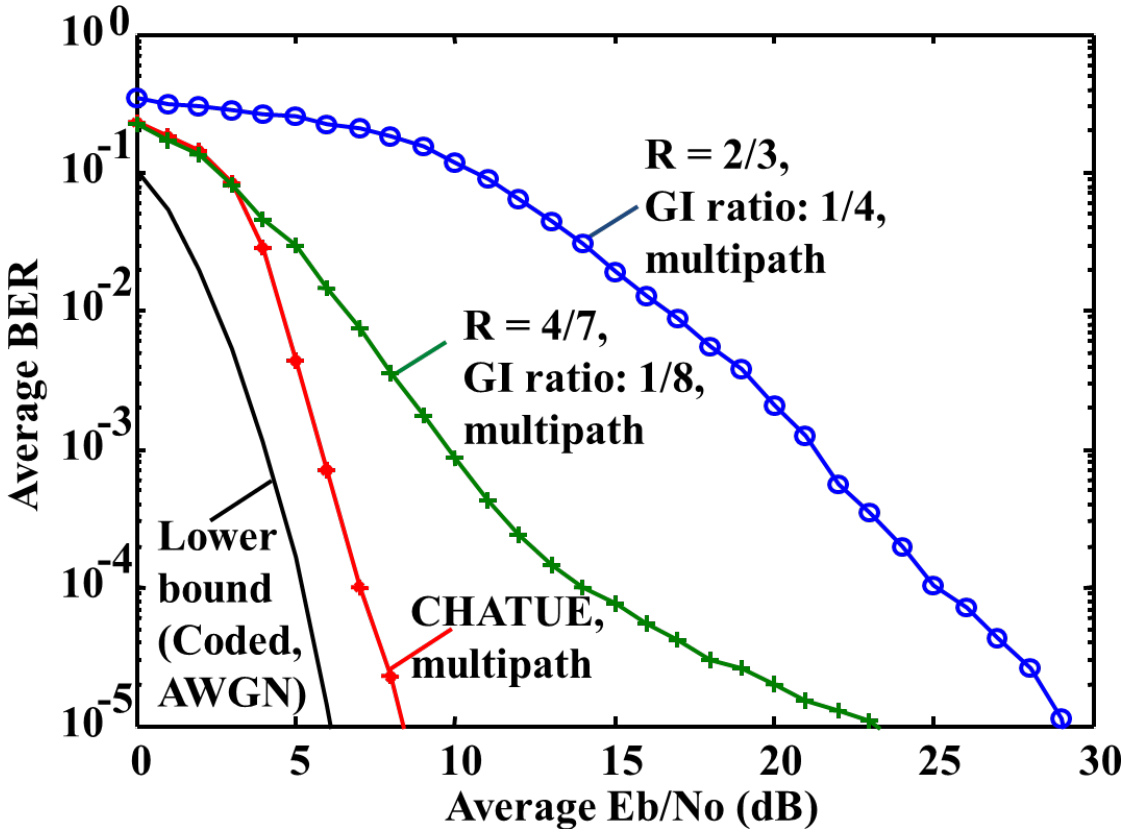

Figure C.1. BER Performance of CHATUE for Single User OFDM

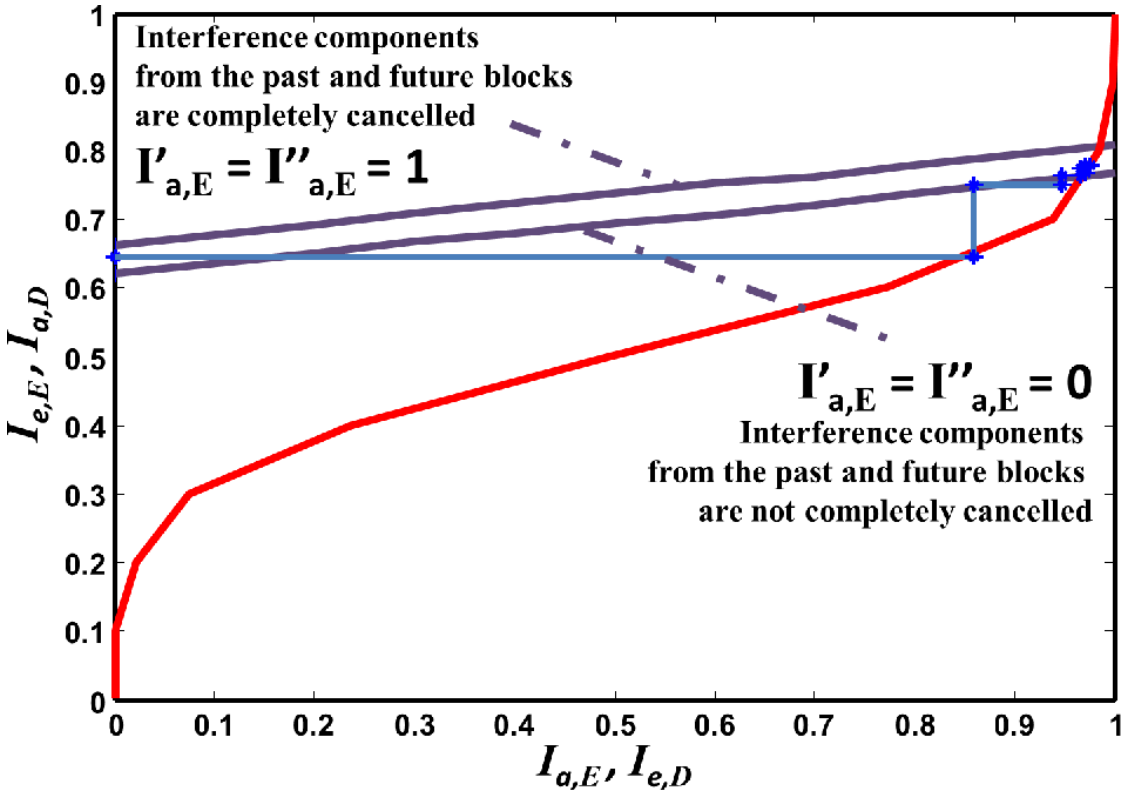

Figure C.2. EXIT Chart of Two Extreme Cases of CHATUE-MU-SIMO-OFDM without $DAcc$ at $\mathrm{E}_b/\mathrm{N}_o = 5$ dB

C.2 Multiuser's Case

In Section C.2, two cases of CHATUE MU-SIMO-OFDM which are having different multipath channel models, COST 207 and 64 paths Jakes models, are considered. The results of EXIT chart analyses and BER performances are provided.

C.2.1 EXIT Analysis

Fig. C.2 and Fig. C.3 show the EXIT curves of the equalizer and the decoder for $\mathrm{E}_b/\mathrm{N}_o = 5$ dB for the systems without $DAcc$ and with $DAcc$, respectively. A half-rate NSNRCC with memory-2 and its generator polynomial $G = [7, 5]$ are considered. For the simplicity, we only plot the lower and upper bound EXIT curves. The lower bound is obtained by setting the MI provided from the equalizers for the past and future blocks to be $I'_{a,E} = I''_{a,E} = 0$, which corresponds to the case where all ISI components remains. Whereas the upper bound is obtained by setting $I'_{a,E} = I''_{a,E} = 1$, which

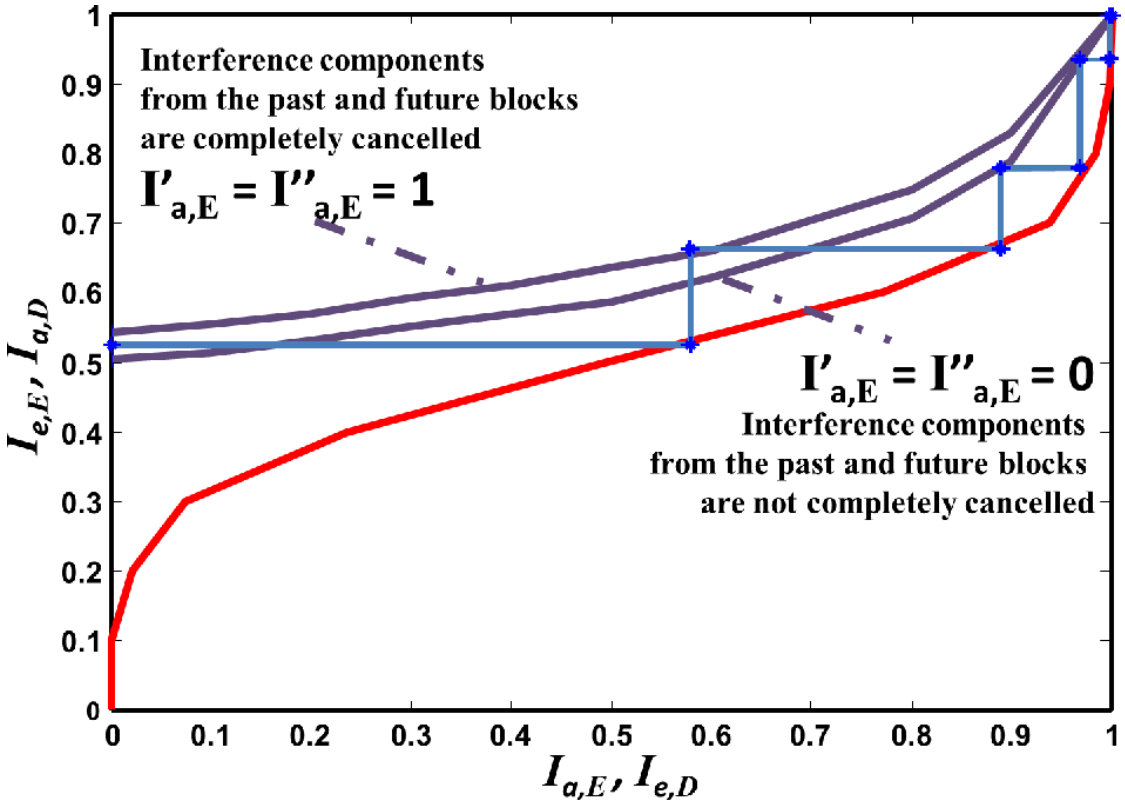

Figure C.3. EXIT Chart of Two Extreme Cases of CHATUE-MU-SIMO-OFDM with $DAcc$ at $\mathrm{E}_b/\mathrm{N}_o = 5$ dB

corresponds to the case where all ISI components are completely cancelled.

A decoding trajectory visualizes the exchange of extrinsic information between constituent soft-input-soft-output (SISO) blocks, which are the equalizer and the channel decoder. A simulation for generating the trajectory line is organized as follows. Three consecutive equalizer blocks are connected in time, i.e. EQ_{t-1}, EQ_t, EQ_{t+1} as the past, the present, and the future blocks, respectively. The MI fed back from the past block, as well as from the future block are set at zero. We start evaluated the MI between the input of channel decoder and the coded bits $\mathbf{b}_c$ of the present block, denotes by $I_{e,E} = I_{a,D}$, iteration-by-iteration. Here the extrinsic MI from the decoder to the EQ_t, denotes by $I_{e,D} = I_{a,E}$, is set at zero as the initial value, afterwards, the step-wise line are drawn by evaluating $I_{e,E}$ and $I_{a,E}$, according to the iterations. The trajectory in the both Fig. C.2 and Fig. C.3 illustrate that no more significant iteration gain is obtained after four iterations.

Fig. C.2 shows the EXIT chart without using $DAcc$ in the systems. It is found

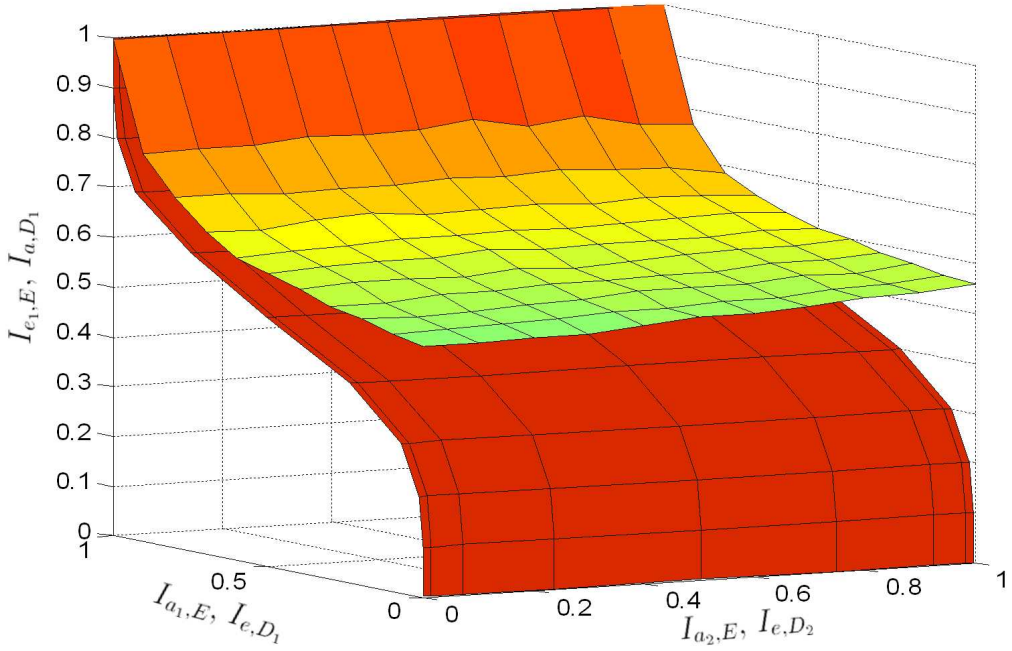

Figure C.4. Three Dimensional EXIT Analysis of CHATUE-MU-SIMO-OFDM with Doped-Accumulator at $\mathrm{E}_b/\mathrm{N}_o = 5$ dB

that with the MI feedback from the past and the future being zero, the EXIT curves intersect each other, which makes the trajectory can not reach the $I_{e,D} = 1$. With the MI from the past and the future block being one, the EXIT curves intersect each other as well. Therefore, we can not reduce the error probability to arbitrarily small.

To avoid this problem, a modification was introduced by exploiting $DAcc$ and adjusting the doping rate p in $DAcc$ to adjust the equalizer EXIT curve so that the convergence tunnel opens up to the (1.0, 1.0) MI point, as shown in the Fig. C.3. In this case, we use $p = 4$ as the doping rate. It is found that a point close enough to the (1.0, 1.0) MI point can be reached without having intersection.

Fig. C.4 shows the three-dimensional (3D) EXIT planes of the $EQ + D_{DAcc}$ for the first user. *A priori* MI I_{a_1} and I_{a_2} are provided by the first and the second users's decoders (Dec_1 and Dec_2, respectively) via their corresponding interleavers (Π_1 and Π_2, respectively). Equalizer's extrinsic MI of the first user is denoted by I_{e_1}. The EXIT plane for the decoder is also plotted. Note that since the both users use identical code in this case, the decoder's EXIT planes are also the same for them. For the sake of

Table C.2. Simulation Parameters of CHATUE-MU-SIMO-OFDM, COST 207 Channel Model

Transmitter	Antenna	$K_T = 2, K_R = 2$
	Modulation	BPSK
	DFT/IDFT size	512
	Encoder	NSNRCC with GP = [5,7]
	Interleaver	Random
	doping rate	4
	CP rate	1/8
Channel	Multipath Selective Fading	rural area (COST 207)
	Multipath Selective Fading	bad urban (COST 207)
Receiver	Equalizer	FD/SC-MMSE
	Iterations	4
	Channel Estimation	Perfect
	Synchronization	Perfect
	Decoder	log-MAP BCJR

simplicity, it is assumed in this figure that the interference components from the past and the future blocks are completely cancelled. It is found from the 3D EXIT chart that the convergence tunnel opens until a point very close to the (1,1) MI point, and the larger the I_{a_2} value (*a priori* information to the equalizer fed back from the second user's decoder, Dec_2), larger the gap of the tunnel. This obviously indicates that the first user's convergence is enhanced with the help of the second user, and vice-versa.

C.2.2 BER Performance

C.2.2.1 COST 207 Channel

Computer simulations were conducted to evaluate the performances, using the parameters shown in table C.2.2.1. All random interleaver length are 512 in bits. For fair comparison, the coding rate was adjusted while keeping the number of the information bits in one block (including the CP length in the case of CP-transmission) constant for the both proposed and the conventional CP-transmission cases.

We use multipath selective fading channel based on the COST 207 channel models [26]. Here, we select rural-area and bad-urban channel models as representative of wide range application to the channel conditions. We use bad-urban channel model for the performance comparison between CP-aided and non-CP-aided transmission scheme. We also assume that the receiver has perfect knowledge about the channel.

Fig. C.5 shows roughly 3 dB gain in E_b/N_0 can be achieved with non-CP-aided

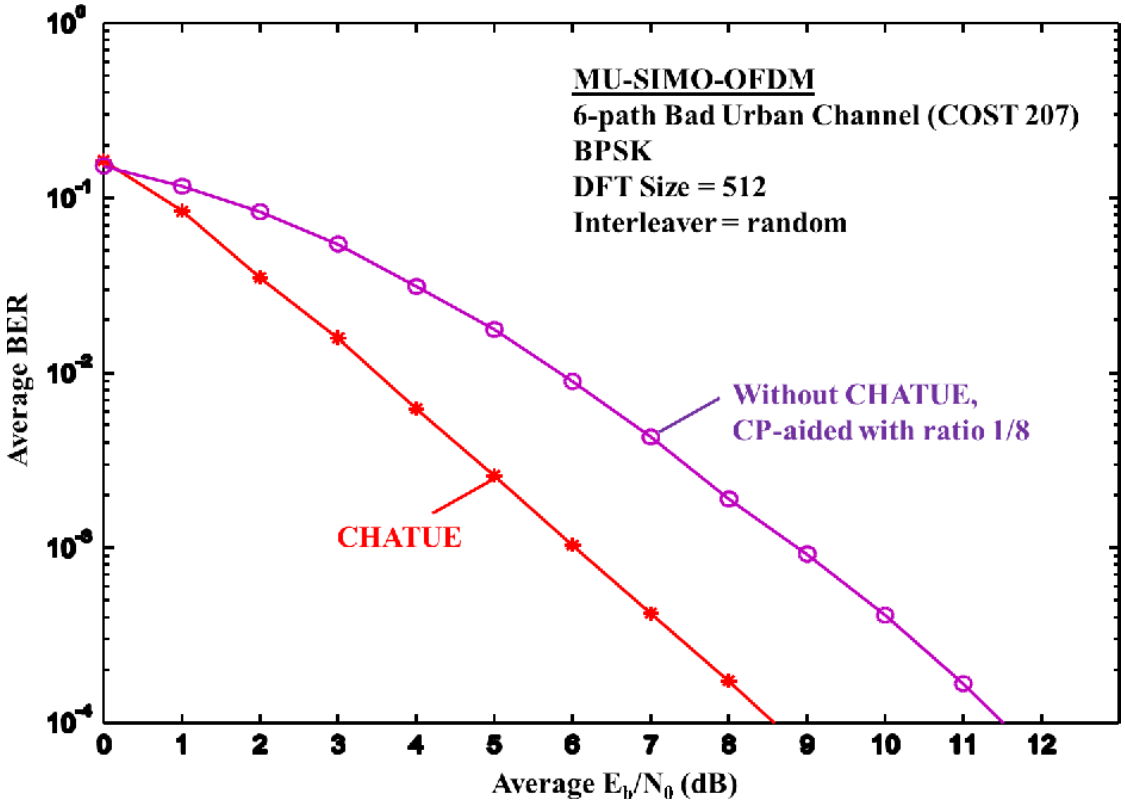

Figure C.5. BER Performance of MU-SIMO-OFDM, with and without CHATUE

transmission at BER $= 10^{-4}$ over the CP-aided transmission scheme. Obviously, the gain is due to the utilization of the strong code (lower rate), made possible by eliminating the CP. The performances of CHATUE in bad-urban and rural-area channel models are shown in Fig. C.6. In general, the more the multipath, the higher the diversity gain, and thereby the CHATUE performance improvement is decreased in rural-areas. However, still in average, about 1.3 dB improvement can be achieved at BER $= 10^{-4}$ by utilizing $DAcc$. These results confirm the analysis that has been shown in the EXIT Chart analysis provided in Subsection C.2.1.

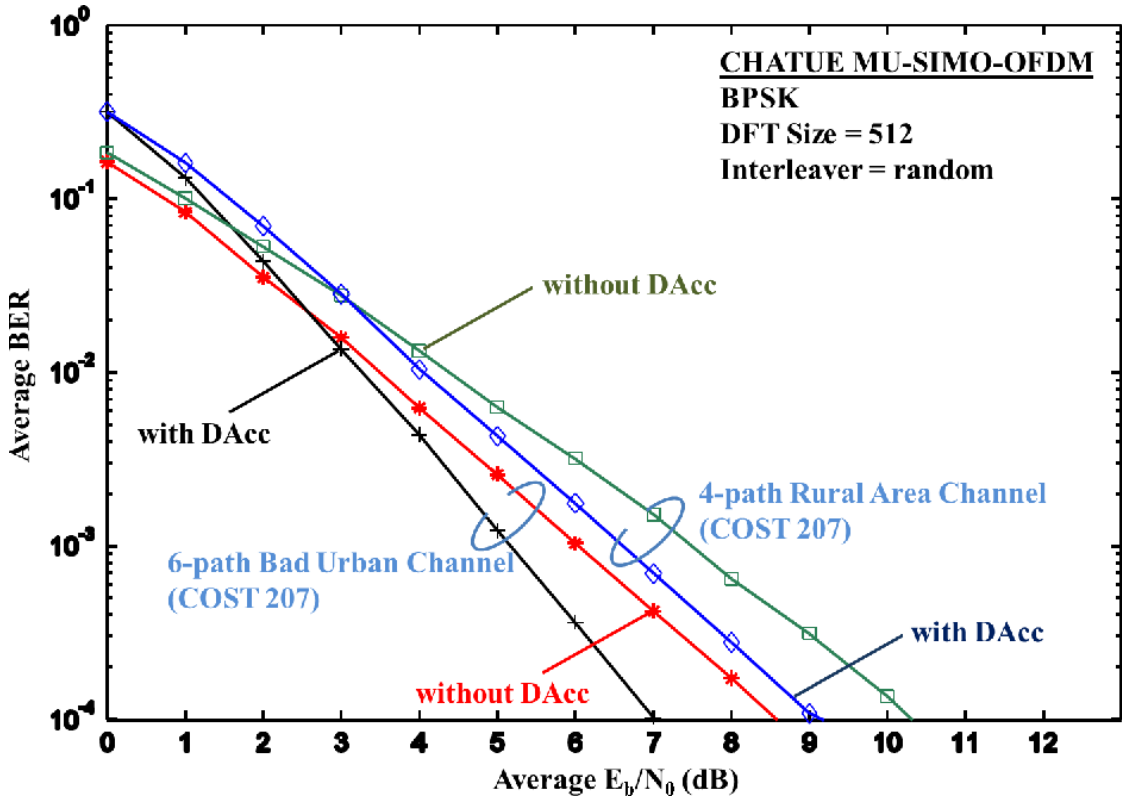

Figure C.6. BER Performance of MU-SIMO-OFDM over COST 207 Channel

Table C.3. Simulation Parameters of CHATUE-MU-SIMO-OFDM, Jakes Model

Transmitter	Antenna	$K_T = 2, K_R = 2$
	Modulation	BPSK
	DFT/IDFT size	512
	Encoder	NSNRCC with GP = [5,7]
	Interleaver	Random
	doping rate	4
Channel	Multipath Fading	64 paths, Jakes Model
Receiver	Equalizer	FD/SC-MMSE
	Iterations	10
	Channel Estimation	Perfect
	Synchronization	Perfect
	Decoder	log-MAP BCJR

C.2.2.2 64 Paths, Jakes Model

In 64-paths Rayleigh fading channel, it can be found that without DAcc, a 2.5 dB gain in E_b/N_0 can be achieved by the CHATUE algorithm at BER = 10^{-5}, and in addition to the 2.5 dB gain, a 3.6 dB gain can be achieved by utilizing DAcc, as shown in Fig. C.7. Obviously, the 2.5 dB gain is due to the utilization of the lower rate (hence more powerful) code, made possible by eliminating the CP, and the additional 3.6 dB gain is due to the fact that the convergence tunnel opens until a point very close to the (1,1) MI point.

When evaluating the lower and upper bounds of the BER of CHATUE with DAcc, we used the same technique as that used in evaluating the trajectories. Also, we used the same technique in the chain simulation conducted to evaluate the BER performance, i.e. *truncation length* = 3, and the MI values of future-of-the-future and past-of-the-past were both set at zero. The results are shown in Fig. C.7. It is found that the BER curve obtained by the real chain simulation is between the bounds.

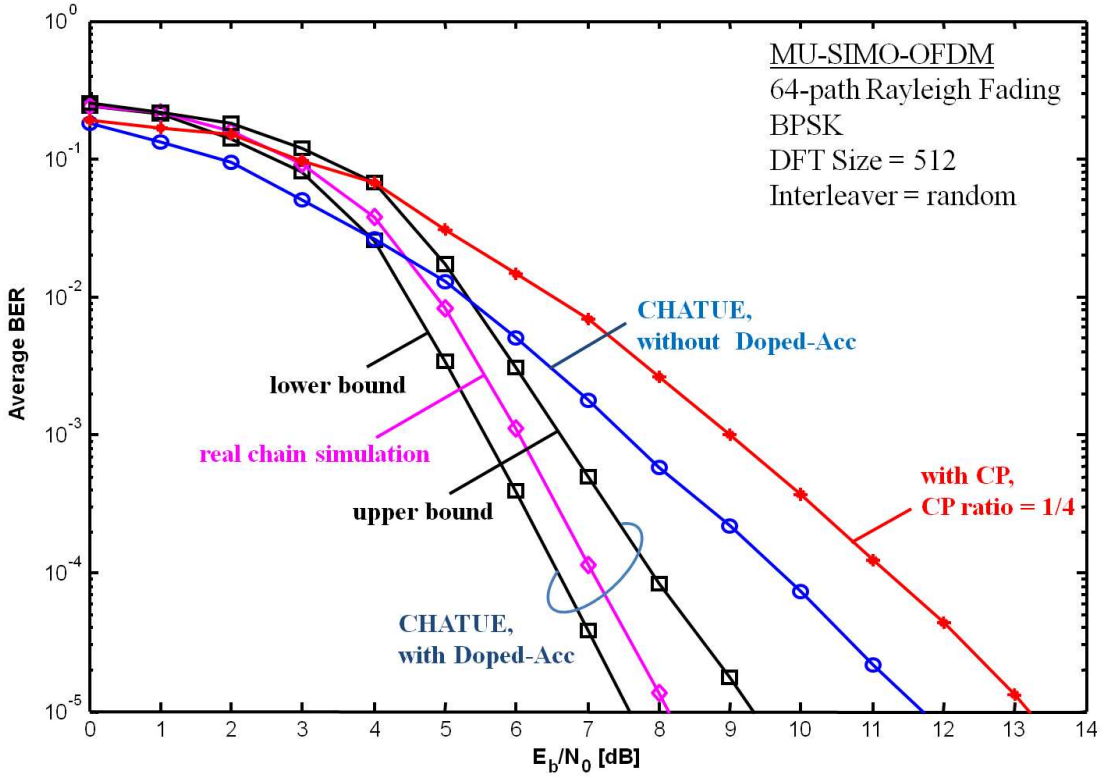

Figure C.7. BER Performance of MU-SIMO-OFDM over 64-paths Fading Channel

Bibliography

[1] Lin, S. and D. Costello (2004) *Error Control Coding: Fundamentals and Applications*, Pearson-Prentice Hall.

[2] Berrou, C., A. Glavieux, and P. Thitimajshima (1993) "Near Shannon limit error-correcting coding and decoding: Turbo-codes," in *Communications, 1993. ICC '93 Geneva. Technical Program, Conference Record, IEEE International Conference on*, vol. 2, pp. 1064–1070.

[3] Narayanan, K. R. and G. L. Stuber (1997) "A Novel ARQ Technique Using the Turbo Coding Principle," *IEEE Commun. Letters*, **1**(2), pp. 49–51.

[4] Souza, R. D., M. E. Pellenz, and T. Rodrigues (2009) "Hybrid ARQ Scheme Based on Recursive Convolutional Codes and Turbo Decoding," *IEEE Trans. on Commun.*, **57**(2), pp. 315–318.

[5] Rowitch, D. N. and L. B. Milstein (2000) "On the Performance of Hybrid FEC/ARQ Systems Using Rate Compatible Punctured Turbo (RCPT) Codes," *IEEE Trans. on Commun.*, **48**(6), pp. 948–959.

[6] Mantha, R. and F. Kschischang (1999) "A capacity-approaching hybrid ARQ scheme using turbo codes," in *Global Telecommunications Conference, 1999. GLOBECOM '99*, vol. 5, pp. 2341 – 2345 vol.5.

[7] Samra, H. and Z. Ding (2005) "A Hybrid ARQ Protocol Using Integrated Channel Equalization," vol. 53, pp. 1996–2001.

[8] Ait-Idir, T. and S. Saoudi (2009) "Turbo Packet Combining Strategies for the MIMO-ISI ARQ Channel," *IEEE Trans. on Commun.*, **57**(12), pp. 3782–3793.

[9] Assimi, A. n., C. Poulliat, and I. Fijalkow (2008) "Packet combining for turbo-diversity in HARQ systems with integrated turbo-equalization," in *2008 5th International Symposium on Turbo Codes and Related Topics*, pp. 61 – 66.

[10] ——— (2009) "Diversity Technique for Single-Carrier Packet Retransmissions over Frequency-Selective Channels," in *Eurasip Journal on Wireless Communications and Networking*, vol. 2009.

[11] G. D. Forney, J. (1965) *Concatenated Codes*, Massachusetts Institute of Technology.
URL http://dspace.mit.edu/bitstream/handle/1721.1/4303/rle-tr-440-04743368.pdf

[12] ten Brink, S. (2001) "Convergence Behavior of iteratively decoded parallel concatenated codes," *IEEE Trans. Comm.*, **49**, pp. 1727–1737.

[13] Brannstrom, F., L. Rasmussen, and A. Grant (2005) "Convergence Analysis and Optimal Scheduling for Multiple Concatenated Codes," *Information Theory, IEEE Transactions on*, **51**(9), pp. 3354–3364.

[14] Sheikh, A. (2004) *Wireless Communications: Theory and Techniques*, Kluwer Academic Pub.

[15] Wicker, S. (1995) *Error control systems for digital communication and storage*, Prentice Hall.

[16] Jakes, W. (1974) *Microwave mobile communications*, IEEE Press classic reissue, IEEE Press.

[17] Pop, M. and N. Beaulieu (2001) "Limitations of sum-of-sinusoids fading channel simulators," *Communications, IEEE Transactions on*, **49**(4), pp. 699–708.

[18] 3GPP (2006) "Technical Specication Group Radio Access Networks Physical layer aspects for evolved Universal Terrestrial Radio Access (UTRA)," *Technical Specication TR 25.814 V7.1.0, Release 7*.

[19] Kansanen, K. and T. Matsumoto (2007) "An analytical method for MMSE MIMO turbo equalizer EXIT chart computation," *Wireless Communications, IEEE Transactions on*, **6**(1), pp. 59–63.

[20] Anwar, K., H. Zhou, and T. Matsumoto (2010) "Chained Turbo Equalization for Block Transmission without Guard Interval," in *IEEE VTC2010-Spring*, Taiwan.

[21] Pfletschinger, S. and F. Sanzi (2006) "Error Floor Removal for Bit-Interleaved Coded Modulation with Iterative Detection," *IEEE Trans. on Wireless Comm.*, **5**(11), pp. 3174–3181.

[22] Wang, D., C. Wei, Z. Pan, X. You, C. H. Kyuu, and J. B. Jang (2008) "Low-complexity Turbo Equalization for Single-Carrier Systems without Cyclic Prefix," in *IEEE ICC*, Beijing, pp. 1091–1095.

[23] Kansanen, K. and T. Matsumoto (2007) "An Analytical Method for MMSE MIMO Turbo Equalizer EXIT Chart Computation," *IEEE Trans. Wireless Comm.*, **6**(1), pp. 59–63.

[24] Bahl, L., J. Cocke, F. Jelinek, and J. Raviv (1974) "Optimal Decoding of Linear Codes for minimizing symbol error rate," *IEEE Trans. on Info. Theory*, **IT-20(2)**, pp. 284–287.

[25] McEliece, R. and W. Lin (1996) "The trellis complexity of convolutional codes," *Information Theory, IEEE Transactions on*, **42**(6), pp. 1855 –1864.

[26] Patzold, M. (2002) *Mobile Fading Channel*, John Wiley & Sons, p. 259.